(polD4-5), and MS551F and MS552R (polD4-3-1) were annealed, then inserted between the restriction sites BglII and HindIII in PH1RNAneo [7]. Cells transfected with a vector carrying either polD4-3-1 or polD4-5 were cultured in media containing 1 mg/ml G418 (Invitrogen, Carlsbad, CA 10131-027), which was reduced by 0.2 mg/ml every 2 days until it reached 0.4 mg/ml. When colonies grew to visible seizes, they were fixed by cold methanol for 5 min and stained with 4% Giemsa for 15 min at room temperature.

RNA interference. Transfection was carried out using 50 nmol/L of a small interfering RNA (siRNA) duplex (Sigma–Aldrich) targeting each mRNA, or negative control 1# (Ambion) with Lipofectamine-2000 (Invitrogen). The sequences of si*POLD4* were the same as those of polD4-3-1: *POLD4* (si*D4*) sense, 5′-GCAUCUCUAUCCCCUAUGATT-3′; and antisense, 5′-UCAUAGGGGAUAGAGAUGCTT.

Laser scanning cytometry (LSC). Following an overnight culture, 3×10^5/ml Calu6 cells on coverslips were fixed by cold methanol, washed with PBS, and incubated with 1 mg/ml RNase A in 50 mM Tris–HCl, pH 7.5, at 37 °C for 1 h. Cells were further treated with 50 μg/ml propidium iodide in a mixture containing 180 mM Tris–HCl, pH 7.5, 180 mM NaCl, and 70 mM $MgCl_2$ for 15 min. Nuclei structures and DNA contents were analyzed using a Laser Scanning Cytometer (LSC, Olympus, Tokyo, Japan), with DNA content at the G1 peak regarded as 2N, though Calu6 cells carry a greater amount of DNA chromatin than normal cells.

Cell cycle synchronization. Calu6 cells were synchronized according to the method of Nakagawa et al. [8], with minor modifications. In brief, 24-h treatment with 2 mM thymidine was used to arrest exponentially proliferating cells in the S phase. Cells were then released from arrest by three washes in PBS and grown in fresh medium for 15 h, then 1 μM of aphidicolin was used for the second block for 10 h. After releasing by three washes in PBS, cells were incubated in RPMI1640 containing 5% fetal bovine serum and harvested at various time points.

Immunofluorescence. Following an overnight culture, 3×10^5/ml Calu6 cells on coverslips were transfected with siRNA as described above. After 48 h, they were fixed in 4% paraformaldehyde for 10 min at room temperature, followed by treatment with cold methanol for 2 min. The coverslips were washed three times in PBS, treated with PBS containing 0.25% Triton X-100 on ice for 30 min, and incubated with anti-lamin B or anti-γ-tubulin antibody overnight at 4 °C. The cells were then washed three times in PBS, incubated for 1 h with Alexa 488-conjugated secondary antibody (Molecular Probes, OR, USA), and analyzed using an Olympus BX60 (Olympus).

Results and discussion

DNA synthesis activities of pol δ with or without POLD4 in vitro

In order to analyze POLD4 functions related to intrinsic pol δ activity, 3- and 4-subunit structures of pol δ were expressed and purified. In the absence of POLD4, pol δ was less active than the holoenzyme in a reaction containing poly dA–dT as a template primer (Fig. 1A), with a similar result obtained when the accessory protein of PCNA was omitted from the reaction (Fig. 1B). These results are consistent with those of previous studies [1,3] and indicate that POLD4 is required for pol δ to exhibit its full catalytic activity.

POLD4 required for cell proliferation

A previous genetic study of *S. pombe* demonstrated that the *POLD4* ortholog of *Cdm1* is a non-essential gene for cell growth,

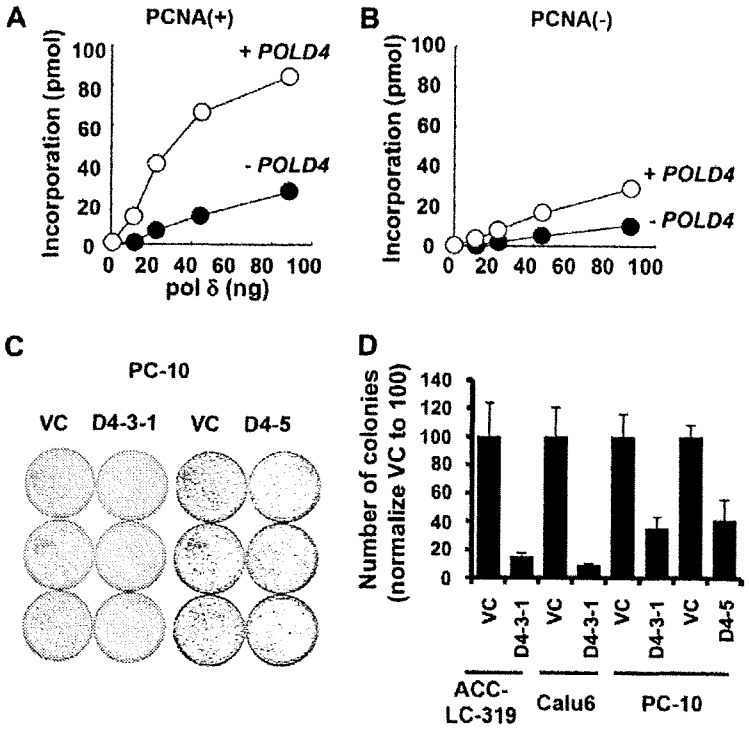

Fig. 1. *In vitro* DNA synthesis activities of pol δ and effect of POLD4 depletion on colony formation activity. (A) pol δ activities were measured and plotted as described in Materials and methods. (B) The same reactions were carried out in the absence of PCNA. (C) PC-10 was used for transfection with plasmids carrying either D4-3-1 or D4-5, and colony formation activity was determined as described in Materials and methods. VC represents vector control. (D) Results of the colony formation assay were plotted in a graph.

division, and sensitivity to DNA damaging reagents [4]. Nevertheless, it is possible that mammalian cells with larger genomic sizes require POLD4 for efficient and accurate DNA replication. We investigated this possibility using shRNA-mediated knockdown of *POLD4*. As shown in Fig. 1C, two independent sequences of shRNA caused reduced activity in a colony formation assay using PC-10, a human non-small cell lung cancer (NSCLC) cell line. Similar results were obtained with different NSCLC cell lines, Calu6 and ACC-LC-319 (Fig. 1D). These findings suggest that human cells require POLD4 for proliferation.

Structure and population of karyomere-like cells following siPOLD4 treatment

Since pol δ is a major DNA replication and repair polymerase, impairment of its activity may cause DNA replication stress, such as accumulation of single-stranded DNA gaps, and inefficient repair of endogenous DNA damage, which ultimately results in cell death. On the other hand, it is also possible that some cells continue to grow following such genetic erosion, which may cause genomic instability. Therefore, we investigated whether POLD4 is also required for suppressing genomic instability in human cells. Initially, we attempted to establish stable clones with low POLD4 expression using shRNA-treated cells. However, clones with adequate levels of POLD4 expression were gradually selected, leading to recovery to the original level over time (data not shown). Therefore, in the following experiments, we used siRNA to transiently reduce POLD4 expression (Fig. 2A, left).

Calu6 cells treated with si*POLD4* formed multiple or lobed nuclei, at a 5.3-fold greater frequency than in the control experiment (Fig. 2B and C). Similar structures were also observed when A549 cells were treated with si*POLD4* (data not shown). Staining with

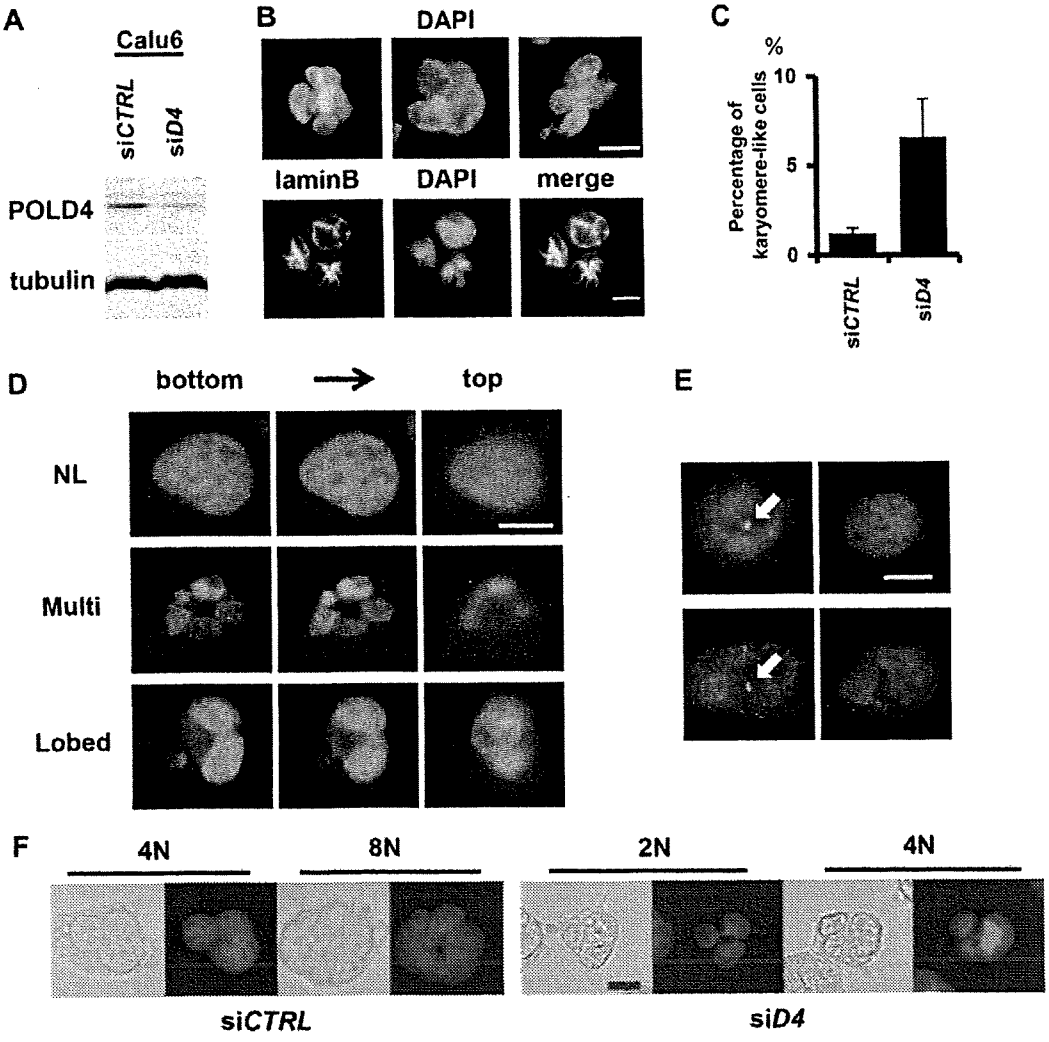

Fig. 2. Structures and population of karyomere-like cells upon si*POLD4* treatment. (A) Western blot analysis of POLD4 and α-tubulin in protein extracts from si*POLD4*- or si*CTRL*-treated Calu6 cells. (B) Upper panels: Calu6 cells were treated with si*POLD4* for 48 h and stained with DAPI. Sample karyomere-like nuclei are shown. Lower panels: Calu6 cells were treated with si*POLD4* for 48 h, then visualized with anti-lamin B antibody or DAPI. (C) Calu6 cells were treated with si*POLD4* or si*CTRL*, then the frequencies of karyomere-like structures in 1000 cells were counted and plotted. In this experiment, cells with three or more nuclear lobes, or three or more nuclei were regarded as karyomere-like cells. Averages of three independent results are shown with SD. (D) si*POLD4*-treated cells were stained by DAPI, then three sequential photographs were taken every 4 μm from the bottom. Upper, middle, and lower panels show images of normal, multiple, and lobed nuclear structures, respectively. (E) After being treated with si*POLD4*, cells were visualized with anti-γ-tubulin (left) or DAPI (right). Upper and lower panels show representative pictures of normal and karyomere-like nuclei, respectively. Centrosomes are indicated by arrows. (F) LSC analysis. Phase-contrast and propidium iodide-stained images of karyomere-like cells among 4N and 8N (si*CTRL*), or 2N and 4N (si*POLD4*) cells. Bar indicates 10 μm.

the anti-lamin B antibody outlined the edges of the DAPI structures and showed that the nuclear envelope was formed around chromatin (Fig. 2B, lower). Sequential acquisition of images from the bottom of the cells further illustrated the abnormal structures of single cells, including a flat profile and multiple nuclei (Fig. 2D, middle panels), or a single nucleus associated with multiple lobes (Fig. 2D, lower panels). For both types of abnormal structures, the nuclear sizes were approximately that of a normally shaped nucleus (Fig. 2D, upper panels).

The multiple nuclei seen with these structures were reminiscent of 'micronuclei' that indicated the presence of DNA damage and DNA replication stress in previous studies [9–11], while the lobed nuclei closely resembled 'karyomere' nuclei observed in zebrafish blastomeres [12] and early *Xenopus laevis* development [13]. In that latter study and other studies referenced therein, it was suggested that karyomere formation is a physiological mitotic process that may share similar mechanisms with pathological micronuclei formation; with both multiple and lobed nuclei, isolated chromosomes might

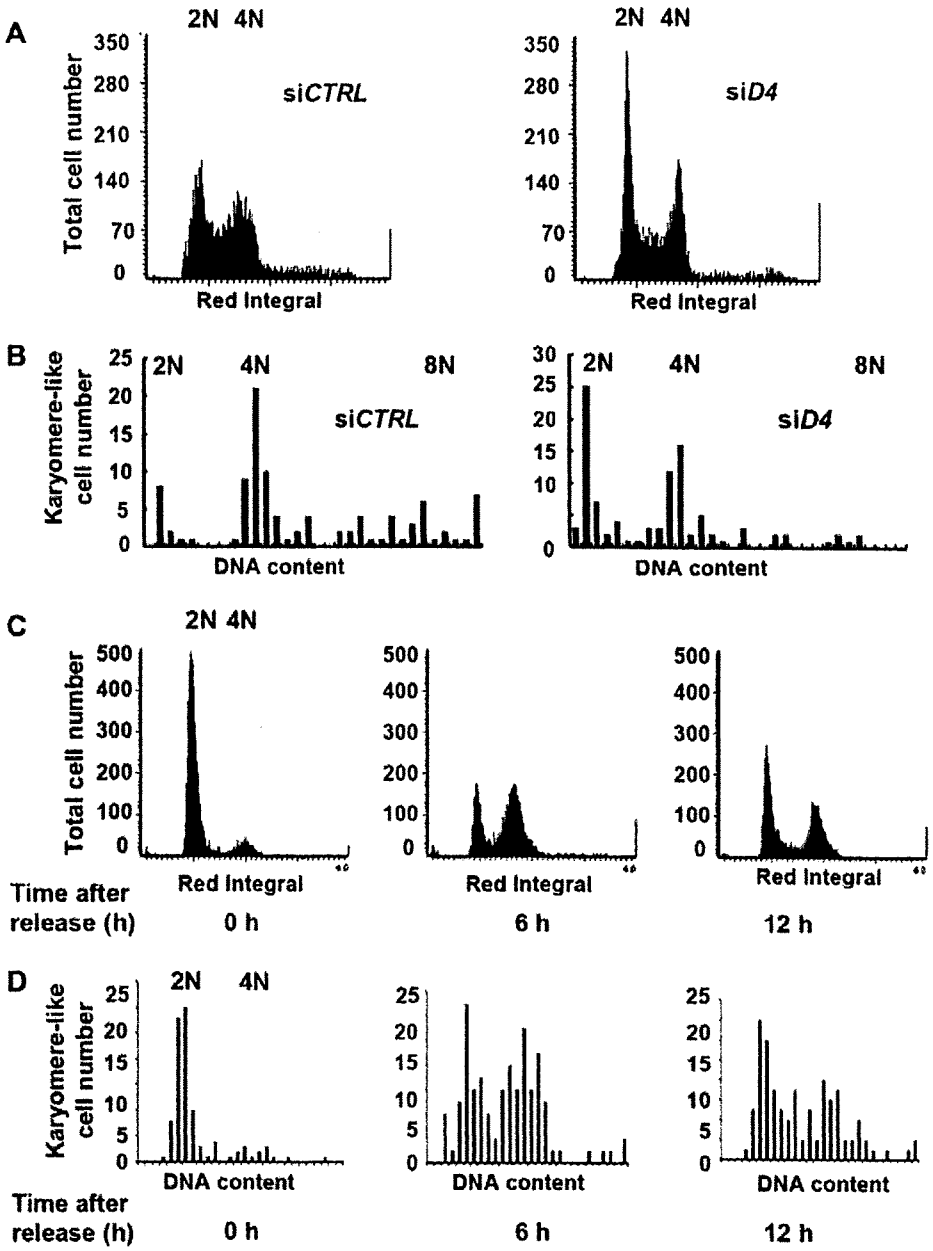

Fig. 3. Cell cycle dynamics of karyomere-like cells. (A) Calu6 cells were treated with si*CTRL* (left) or si*POLD4* (right), then their DNA contents were subjected to LSC analysis. The G1 population found among the majority of cells was regarded as 2N. (B) In the same experiment, DNA contents of 100 karyomere-like cells were determined. Cell numbers in each DNA content range were plotted with histograms. (C) Calu6 cells were treated with si*POLD4*, then synchronized at the G1/S boundary and released for cell cycle progression. At 0, 6, or 12 h after release, DNA contents were subjected to LSC. (D) In the same experiment, the DNA contents of 100 karyomere-like cells were measured. Cell numbers in each DNA content range were plotted with histograms.

be surrounded by a nuclear envelope after chromosome segregation occurs. Therefore, those two types of abnormal structures are referred to as karyomere-like nuclei hereafter.

In addition to DNA damage, formation of karyomere-like nuclei may also occur as a consequence of dysfunctions of the mitotic apparatus [13,14]. Moreover, a previous study found that the anti-POLD4 antibody bound the surface of mitotic chromosomes, which suggests specific functions of POLD4 during mitosis [5]. To investigate this, we analyzed the centrosome structures in si *POLD4*-treated cells, as it has been reported that disturbed chromosomal migration occurred with abnormal replication or localization of centrosomes [15,16]. Our present results showed that si *POLD4*-treated cells were associated with normal centrosome structures, which had one or two centrosomes located at a single site (Fig. 2E). We also quantified the lagging-chromosome frequencies, and found that they were very similar between si*POLD4*- and si*CTRL*-treated mitotic cells (data not shown). Although the results of this limited experiment were contrary to our speculation that POLD4 has some mitotic functions, we intend to conduct more detailed examinations in the future.

Cell cycle dynamics of karyomere-like cells

In the following experiments, we studied the cell cycle dynamics of karyomere-like cells. After si*POLD4* treatment, we observed checkpoint activation (data not shown, detailed mechanisms discussed elsewhere), and accumulations of G1- and G2-populations (Fig. 3A). In si*CTRL*-treated cells, most of the karyomere-like populations were found among the minor aneuploid populations (Figs. 3B and 2F, left panels). In contrast, karyomere-like cells in si *POLD4*-treated cells were found to have normal ploidy as seen with 2N–4N cells (Fig. 3B, 2F, right panels).

In order to determine if karyomere-like cells remained alive and had an ability to progress through the cell cycle, we synchronized cells at the G1–S boundary, then released them and observed the cell cycle progression, as well as the associated nuclear shapes (Fig. 3C–E). Interestingly, karyomere-like cells progressed through the cell cycle and returned to G1 at 12 h after release. In support of these results, most karyomere-like cells were negative in TUNEL staining findings (data not shown). Therefore, these structures may not reflect the pro-apoptotic phenotype. Our results suggest that most karyomere-like cells are able to proliferate until they became arrested at the G1 or G2 phase, when DNA damage reaches an intolerant level.

In conclusion, our results showed that POLD4 supports cellular proliferation and suppresses karyomere-like nuclei formation in human cells, which might occur as a consequence of impairment of the DNA replication and repair activities of pol δ. A future study to identify the direct link between POLD4 and mitotic functions may reveal the underlying mechanisms to maintain genomic stability in human cells.

Acknowledgments

We thank Keiko Ueda and Makiko Terada for their initial involvement in this project. We are also grateful for Dr. Takeshi Senga of our university for the critical reading of the manuscript. This work was supported in part by a Grant-in-Aid for Scientific Research on Innovative Areas, a Grant-in-Aid for Scientific Research on Priority Areas from the Ministry of Education, Culture, Sports, Science, and Technology of Japan, and a Grant-in-Aid for Scientific Research from the Japan Society for the Promotion of Science.

References

[1] V.N. Podust, L.S. Chang, R. Ott, G.L. Dianov, E. Fanning, Reconstitution of human DNA polymerase delta using recombinant baculoviruses: the p12 subunit potentiates DNA polymerizing activity of the four-subunit enzyme, J. Biol. Chem. 277 (2002) 3894–3901.
[2] L. Liu, J. Mo, E.M. Rodriguez-Belmonte, M.Y. Lee, Identification of a fourth subunit of mammalian DNA polymerase delta, J. Biol. Chem. 275 (2000) 18739–18744.
[3] H. Li, B. Xie, Y. Zhou, A. Rahmeh, S. Trusa, S. Zhang, Y. Gao, E.Y. Lee, M.Y. Lee, Functional roles of p12, the fourth subunit of human DNA polymerase delta, J. Biol. Chem. 281 (2006) 14748–14755.
[4] N. Reynolds, A. Watt, P.A. Fantes, S.A. MacNeill, Cdm1, the smallest subunit of DNA polymerase d in the fission yeast *Schizosaccharomyces pombe*, is non-essential for growth and division, Curr. Genet. 34 (1998) 250–258.
[5] P. Dell'Era, S. Nicoli, G. Peri, M. Nieddu, M.G. Ennas, M. Presta, FGF2-induced upregulation of DNA polymerase-delta p12 subunit in endothelial cells, Oncogene 24 (2005) 1117–1121.
[6] Y. Masuda, M. Suzuki, J. Piao, Y. Gu, T. Tsurimoto, K. Kamiya, Dynamics of human replication factors in the elongation phase of DNA replication, Nucleic Acids Res. 35 (2007) 6904–6916.
[7] H. Tanaka, K. Yanagisawa, K. Shinjo, A. Taguchi, K. Maeno, S. Tomida, Y. Shimada, H. Osada, T. Kosaka, H. Matsubara, T. Mitsudomi, Y. Sekido, M. Tanimoto, Y. Yatabe, T. Takahashi, Lineage-specific dependency of lung adenocarcinomas on the lung development regulator TTF-1, Cancer Res. 67 (2007) 6007–6011.
[8] T. Nakagawa, Y. Hayashita, K. Maeno, A. Masuda, N. Sugito, H. Osada, K. Yanagisawa, H. Ebi, K. Shimokata, T. Takahashi, Identification of decatenation G2 checkpoint impairment independently of DNA damage G2 checkpoint in human lung cancer cell lines, Cancer Res. 64 (2004) 4826–4832.
[9] N. Holland, C. Bolognesi, M. Kirsch-Volders, S. Bonassi, E. Zeiger, S. Knasmueller, M. Fenech, The micronucleus assay in human buccal cells as a tool for biomonitoring DNA damage: the HUMN project perspective on current status and knowledge gaps, Mutat. Res. 659 (2008) 93–108.
[10] J.B. Bae, S.S. Mukhopadhyay, L. Liu, N. Zhang, J. Tan, S. Akhter, X. Liu, X. Shen, L. Li, R.J. Legerski, Snm1B/Apollo mediates replication fork collapse and S phase checkpoint activation in response to DNA interstrand cross-links, Oncogene 27 (2008) 5045–5056.
[11] D.J. Kirkland, L. Henderson, D. Marzin, L. Muller, J.M. Parry, G. Speit, D.J. Tweats, G.M. Williams, Testing strategies in mutagenicity and genetic toxicology: an appraisal of the guidelines of the European Scientific Committee for Cosmetics and Non-Food Products for the evaluation of hair dyes, Mutat. Res. 588 (2005) 88–105.
[12] V.K. Schoft, A.J. Beauvais, C. Lang, A. Gajewski, K. Prufert, C. Winkler, M.A. Akimenko, M. Paulin-Levasseur, G. Krohne, The lamina-associated polypeptide 2 (LAP2) isoforms beta, gamma and omega of zebrafish: developmental expression and behavior during the cell cycle, J. Cell Sci. 116 (2003) 2505–2517.
[13] J.M. Lemaitre, G. Geraud, M. Mechali, Dynamics of the genome during early *Xenopus laevis* development: karyomeres as independent units of replication, J. Cell Biol. 142 (1998) 1159–1166.
[14] M. Ohsugi, K. Adachi, R. Horai, S. Kakuta, K. Sudo, H. Kotaki, N. Tokai-Nishizumi, H. Sagara, Y. Iwakura, T. Yamamoto, Kid-mediated chromosome compaction ensures proper nuclear envelope formation, Cell 132 (2008) 771–782.
[15] D. Eriksson, P.O. Lofroth, L. Johansson, K.A. Riklund, T. Stigbrand, Cell cycle disturbances and mitotic catastrophes in HeLa Hep2 cells following 2.5 to 10 Gy of ionizing radiation, Clin. Cancer Res. 13 (2007) 5501s–5508s.
[16] H. Dodson, E. Bourke, L.J. Jeffers, P. Vagnarelli, E. Sonoda, S. Takeda, W.C. Earnshaw, A. Merdes, C. Morrison, Centrosome amplification induced by DNA damage occurs during a prolonged G2 phase and involves ATM, EMBO J. 23 (2004) 3864–3873.

THE JOURNAL OF BIOLOGICAL CHEMISTRY VOL. 284, NO. 38, pp. 25585–25592, September 18, 2009

Translesional DNA Synthesis through a C8-Guanyl Adduct of 2-Amino-1-methyl-6-phenylimidazo[4,5-*b*]pyridine (PhIP) *in Vitro*

REV1 INSERTS dC OPPOSITE THE LESION, AND DNA POLYMERASE κ POTENTIALLY CATALYZES EXTENSION REACTION FROM THE 3′-dC TERMINUS[*S]

Received for publication, June 25, 2009, and in revised form, July 16, 2009 Published, JBC Papers in Press, July 23, 2009, DOI 10.1074/jbc.M109.037259

Hirokazu Fukuda[‡], Takeji Takamura-Enya[§], Yuji Masuda[¶], Takehiko Nohmi[‖], Chiho Seki[‡], Kenji Kamiya[¶], Takashi Sugimura[‡], Chikahide Masutani[**], Fumio Hanaoka[1], and Hitoshi Nakagama[‡2]**

*From the [‡]Biochemistry Division, National Cancer Center Research Institute, 1-1, Tsukiji 5, Chuo-ku, Tokyo 104-0045, the [§]Department of Applied Chemistry, Faculty of Engineering, Kanagawa Institute of Technology, Ogino 1030, Atsugi, Kanagawa 243-0292, the [¶]Department of Experimental Oncology, Research Institute for Radiation Biology and Medicine, Hiroshima University, Kasumi 1-2-3, Minami-ku, Hiroshima, Hiroshima 734-8553, the [‖]Division of Genetics and Mutagenesis, National Institute of Health Sciences, Kamiyoga 1-18-1, Setagaya-ku, Tokyo 158-8501, and the **Cellular Biology Laboratory, Graduate School of Frontier Biosciences, Osaka University, Yamada-oka 1-3, Suita, Osaka 565-0871, Japan*

2-Amino-1-methyl-6-phenylimidazo[4,5-*b*]pyridine (PhIP) is the most abundant heterocyclic amine in cooked foods, and is both mutagenic and carcinogenic. It has been suspected that the carcinogenicity of PhIP is derived from its ability to form DNA adducts, principally dG-C8-PhIP. To shed further light on the molecular mechanisms underlying the induction of mutations by PhIP, *in vitro* DNA synthesis analyses were carried out using a dG-C8-PhIP-modified oligonucleotide template. In this template, the dG-C8-PhIP adduct was introduced into the second G of the TCC GGG AAC sequence located in the 5′ region. This represents one of the mutation hot spots in the rat *Apc* gene that is targeted by PhIP. Guanine deletions at this site in the *Apc* gene have been found to be preferentially induced by PhIP in rat colon tumors. DNA synthesis with A- or B-family DNA polymerases, such as *Escherichia coli* polymerase (pol) I and human pol δ, was completely blocked at the adducted guanine base. Translesional synthesis polymerases of the Y-family, pol η, pol ι, pol κ, and REV1, were also used for *in vitro* DNA synthesis analyses with the same templates. REV1, pol η, and pol κ were able to insert dCTP opposite dG-C8-PhIP, although the efficiencies for pol η and pol κ were low. pol κ was also able to catalyze the extension reaction from the dC opposite dG-C8-PhIP, during which it often skipped over one dG of the triple dG sequence on the template. This slippage probably leads to the single dG base deletion in colon tumors.

Heterocyclic amines (HCAs)[3] are naturally occurring genotoxic carcinogens produced from cooking meat (1). The initial carcinogenic event induced by HCAs is metabolic activation and subsequent covalent bond formation with DNA (1, 2). 2-Amino-1-methyl-6-phenylimidazo[4,5-*b*]pyridine (PhIP) is the most abundant heterocyclic amine in cooked foods, and was isolated from fried ground beef (3, 4). PhIP possesses both mutagenic and carcinogenic properties (5–8). Epidemiological studies have revealed that a positive correlation exists between PhIP exposure and mammary cancer incidence (9). PhIP induces colon and prostate cancers in male rats and breast cancer in female rats (8, 10).

The incidences of colon, prostate, and breast cancers are steadily increasing in Japan and other countries and this has been found to correlate with a more Westernized lifestyle. Elucidating the molecular mechanisms underlying PhIP-induced mutations is therefore of considerable interest. It is suspected that the carcinogenicity of PhIP is derived from the formation of DNA adducts, principally dG-C8-PhIP (11–14) (see Fig. 1). Studies of the mutation spectrum of PhIP in mammalian cultured cells and transgenic animals have revealed that G to T transversions are predominant and that guanine deletions from G stretches, especially from the 5′-GGGA-3′ sequence, are significant (15–20). Five mutations in the *Apc* gene were detected in four of eight PhIP-induced rat colon tumors, and all of these mutations involved a single base deletion of guanine from 5′-GGGA-3′ (21). These mutation spectra are thought to be influenced by various factors, including the primary structure of the target gene itself, the capacity of translesional DNA polymerases, and the activity level of repair enzymes (1). However, the molecular mechanisms underlying the formation of PhIP-induced mutations are largely unknown.

To shed further light on the molecular processes that underpin the mutations induced by PhIP, we performed *in vitro* DNA synthesis analyses using a dG-C8-PhIP-modified oligonucleotide template. We have recently reported the successful synthesis of oligonucleotides harboring a site-specific PhIP adduct

* This work was supported by Kakenhi Grant 19570144.
[S] The on-line version of this article (available at http://www.jbc.org) contains supplemental Table S1 and Figs. S1–S6.
[1] Present address: Dept. of Life Science, Faculty of Science, Gakushuin University, Mejiro 1-5-1, Toshima-ku, Tokyo 171-8588, Japan.
[2] To whom correspondence should be addressed. Tel.: 81-3-3542-2511; Fax: 81-33542-2530; E-mail: hnakagam@ncc.go.jp.
[3] The abbreviations used are: HCA, heterocyclic amines; PhIP, 2-amino-1-methyl-6-phenylimidazo[4,5-*b*]pyridine; TLS, translesional DNA synthesis; IQ, 2-amino-3-methylimidazo[4,5-*f*]quinoline; pol, DNA polymerase; DTT, dithiothreitol; PCNA, proliferating cell nuclear antigen; PIPES, 1,4-piperazinediethanesulfonic acid.

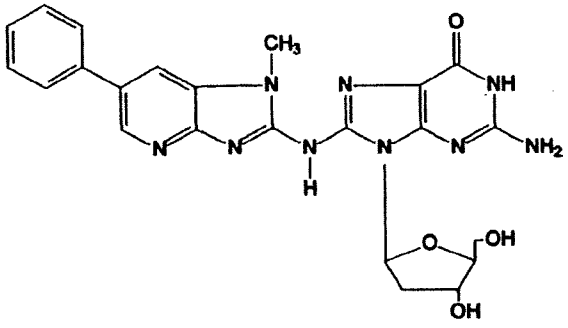

dG-C8-PhIP

FIGURE 1. **Structure of the dG-C8-PhIP adduct.**

(22). In our current study, we used this synthesis method to construct a 32-mer oligonucleotide template containing a 5′-TTCGGGAAC-3′ sequence with different site-specific PhIP adducts. We then utilized the resulting constructs in DNA synthesis analyses to reconstitute the PhIP-induced mutagenesis of the rat *APC* gene. DNA synthesis reactions with A- or B-family DNA polymerases, such as *Escherichia coli* pol I and human pol δ, or translesional synthesis (TLS) polymerases of the Y-family, pol η, pol ι, pol κ, and REV1, were carried out. Kinetic analyses of pol κ and REV1, for which TLS activities at the PhIP adduct were detected, were also performed.

EXPERIMENTAL PROCEDURES

Enzymes and Materials—T4 polynucleotide kinase and T4 DNA ligase were purchased from Toyobo Biochem (Osaka, Japan) and Takara Biotech (Tokyo Japan), respectively. Other materials were obtained from Sigma or Wako (Osaka, Japan).

DNA Polymerases and PCNA—Human recombinant DNA polymerases, pol δ, pol η, pol κ, and REV1, and PCNA were expressed and purified as described previously (23–27). Human DNA polymerase α and DNA polymerase ι were purchased from Chimerx. *E. coli* DNA polymerases I (Takara Biotech) and Klenow Fragment (Takara Biotech), and thermophilic bacterial DNA polymerases, r*Taq* (Toyobo Biochem) and *Tth* (Toyobo Biochem) were used.

Oligonucleotides—The method used to chemically synthesize three 9-mer oligonucleotides, 5′-TCCGGGAAC-3′, containing a PhIP adduct on either the first, second, or third G (p9B, p9C, and p9D, respectively) has been described previously (22). All other synthetic oligonucleotides were synthesized and purified using a reverse-phase cartridge (Operon Biotech Japan (Tokyo, Japan). The 23-mer oligonucleotides: p23a, 5′-TGACTCGTCGTGACTGGGAAAAC-3′, and p23b, 5′-GTCACGACGAGTCAGTTCCCGGA-3′, were used for constructing the template oligonucleotides as described below. A 32-mer oligonucleotide without the PhIP adduct, p32A, was used as a control template (see Table 1). Its 3′ complementary 29-, 28-, 27-, 26-, 22-, and 17-mer sequences (p29, p28, p27, p26, p22, and p17) were used as extension primers (see Table 1).

Construction of Template-Primer Complexes Containing the PhIP Adduct—A 32-mer template oligonucleotide p32C (see Table 1) was constructed by ligation of p9C with p23a as follows. The 5′-end of p23a was phosphorylated by T4 polynucleotide kinase and ATP. A mixture of p9C, p23a, and p23b (3 nmol each) in 250 μl of a buffer containing 5 mM Tris-HCl, 0.5 mM EDTA, 50 mM NaCl, pH 8.0, was denatured for 5 min at 95 °C, incubated for 10 min at 60 °C, and then cooled slowly to form the partial duplex structure of these three oligonucleotides (supplemental Fig. S1). The sample of the duplex oligonucleotide was mixed with 190 μl of Milli-Q water and 50 μl of ×10 ligation buffer (500 mM Tris-HCl (pH 7.5), 100 mM $MgCl_2$, 100 mM DTT, 10 mM ATP). Ligation was initiated by adding 10 μl of T4 DNA ligase (4,000 units), and the mixture was then incubated for 20 h at 16 °C. An additional incubation at 37 °C for 60 min was carried out after the addition of 1 μl of T4 DNA ligase, and the reaction was stopped by further incubation at 68 °C for 10 min. The p32C was separated by 18% PAGE containing 8 M urea, and excised and eluted as described previously (28). p32B and p32D were constructed using a similar method as for p9B and p9D, respectively (see Table 1). The purities of these oligonucleotides, p32B, p32C, and p32D, were determined by denatured PAGE after 5′-end labeling and UV absorbance at 260 and 370 nm.

Primer oligonucleotides were labeled with ^{32}P at the 5′-end as described previously (29), and then purified by MicroSpin™ G-25 or G-50 columns (GE Healthcare) as recommended by the supplier. The mixture of template and labeled primer (50 pmol each) in 400 μl of a buffer containing 8 mM Tris-HCl, 0.8 mM EDTA, 150 mM KCl (pH 8.0) was heated at 70 °C for 7 min, and then cooled slowly to room temperature. In the case of the substrates for TLS polymerases, pol η, pol ι, pol κ, and REV1, the final concentrations of template-primer and the constituents of the annealing buffers were changed to 500 nM and 10 mM Tris-HCl, 1 mM EDTA, and 50 mM NaCl (pH 8.0), respectively.

In Vitro DNA Synthesis Assay—A primer extension reaction was performed as described previously (30) with some modifications. Briefly, an aliquot of 0.75 μl of this primer-annealed template (final concentration, 12.5 nM) was mixed with 0.75 μl of ×10 Klenow buffer (100 mM Tris-HCl (pH 7.5), 70 mM $MgCl_2$, 1 mM DTT), 0.5 μl of 500 mM KCl, 0.5 μl of dNTP mixture (50 μM each), and 4.5 μl of Milli-Q water. After addition of 0.5 μl of Klenow fragment, the mixture was incubated at 37 °C for 10 min. The reaction was terminated by adding 1.5 μl of stop solution (160 mM EDTA, 0.7% SDS, 6 mg/ml proteinase K), and the samples were incubated at 37 °C for 30 min. Subsequently, 5.5 μl of the gel loading solution (30 mM EDTA, 0.05% bromophenol blue, 0.05% xylene cyanol, 97% formamide) was added to the samples. For pol δ, a ×10 reaction buffer containing 200 mM PIPES (pH 6.8), 20 mM $MgCl_2$, 10 mM 2-mercaptethanol, 200 μg/ml bovine serum albumin, and 50% glycerol was used instead of the buffer described above, and the reaction was carried out at 37 °C for 10 min. For other DNA polymerases, pol α, pol I, r*Taq*, and *Tth*, the constituent of each ×10 reaction buffer was altered as recommended by the suppliers.

The reaction using pol κ was performed as described above with some modifications. Briefly, an aliquot of 0.5 μl of this primer-annealed template (final 50 nM) was mixed with 0.5 μl of 10 × TLS buffer (250 mM Tris-HCl (pH 7.0), 50 mM $MgCl_2$, 50 mM DTT, 1 mg/ml bovine serum albumin), 0.5 μl of dNTP solution, and 3.0 μl of Milli-Q water. After addition of 0.5 μl of pol κ, the mixture was incubated at 30 °C for 20 min. The reac-

tion was terminated by adding 8.8 μl of the gel loading solution and a further incubation at 95 °C for 3 min. The reaction of REV1 was performed in the same manner as the reaction of pol κ with the exception that the standard reaction time was 5 min. For pol η, a ×10 reaction buffer containing 400 mM Tris-HCl (pH 8.0), 10 mM $MgCl_2$, 100 mM DTT, 1 mg/ml bovine serum albumin, and 450 mM KCl was used instead of the ×10 TLS buffer. The ^{32}P-labeled fragments were denatured and electrophoresed in a 9.5% polyacrylamide gel containing 8 M urea. The radioactivity of the fragments was determined using a Bio-Imaging Analyzer (BAS2500, Fuji Photo Film, Kanagawa, Japan). Kinetic parameters were determined by steady-state gel kinetic assays under similar conditions as described above. The incubation time for pol κ was changed to 10 min. K_m and k_{cat} were evaluated from the plot of the initial velocity *versus* the dCTP or dGTP concentration using a hyperbolic curve-fitting program in SigmaPlot 11 (Systat Software, Inc.). Data from two or three independent experiments were plotted together.

RESULTS

Construction of Template Oligonucleotides Containing a PhIP Adduct—We designed oligonucleotides containing a dG-C8-PhIP adduct at specific sites for use as templates in *in vitro* DNA synthesis analyses. For this purpose, we selected the 5′-TCCGGGAAC-3′ sequence as: 1) it corresponds to codon 868–870 of the rat *Apc* gene, one of three mutation hot spots (a single base deletion of G) in PhIP-induced colon tumors (21), and could thus be used as a model template that would reconstitute mutations of this gene; 2) two other mutation hot spots in the rat *Apc* gene and many mutated sites induced by PhIP in cultured cells and animal models contain 5′-GGGA-3′ as a core sequence (17–20). We thus speculated that the 5′-TCCGGGAAC-3′ sequence could be used as a model sequence for these GGGA to GGA mutations to some extent; and 3) some mutagenic compounds forming dG adducts, including PhIP, are expected to react preferentially with the 5′-G of a GG dinucleotide site when compared with a single G residue (31). We thus selected a sequence containing GGG as a template for our initial analysis.

We have recently synthesized three 9-mer oligonucleotides separately harboring a PhIP adduct on each G within the sequence 5′-TCC GGG AAC-3′ (22). Three 32-mer template oligonucleotides, p32B, p32C, and p32D, were constructed in our present study by ligation of these 9-mer oligonucleotides containing the dG-PhIP adduct with a 23-mer oligonucleotide, p23a, (Table 1 and supplemental Fig. S1). The purities of these oligonucleotides were tested after resolution by electrophoresis. In our present study, we principally describe the results of our *in vitro* DNA synthesis analysis using p32C as the template to avoid complexity.

In Vitro DNA Synthesis by A- and B-family DNA Polymerase—Many of the chemical compounds that can form DNA adducts *in vivo* and that show mutagenicity have been reported to impede the progress of DNA synthesis to different extents. The molecular size of PhIP is greater than most other mutagenic chemicals that form adducts. Hence, dG-PhIP was expected to block DNA synthesis to a considerable extent. To examine the effects of the dG-C8-PhIP adduct upon DNA synthesis, primer

TABLE 1
Oligonucleotide templates and primers

Oligonucleotide	Sequence[a]
p32A	5′-TCC GGG AAC TGACTCGTC GTGACTGGG AAAAC-3′
p32B	5′-TCC **G**GG AAC TGACTCGTC GTGACTGGG AAAAC-3′
p32C	5′-TCC G**G**G AAC TGACTCGTC GTGACTGGG AAAAC-3′
p32D	5′-TCC GG**G** AAC TGACTCGTC GTGACTGGG AAAAC-3′
p29	5′-GTT TTC CCA GTCACGACG AGTCAGTTC CC-3′
p28	5′-GTT TTC CCA GTCACGACG AGTCAGTTC C-3′
p27	5′-GTT TTC CCA GTCACGACG AGTCAGTTC-3′
p26	5′-GTT TTC CCA GTCACGACG AGTCAGTT-3′
p22	5′-GTT TTC CCA GTCACGACG AGTC-3′
p17	5′-GTT TTC CCA GTCACGAC-3′

[a] The bold G indicates the site of the PhIP-C8-dG adduct. Underlined sequences correspond to codon 868–870 at nucleotides 2602–2610 of the rat APC gene.

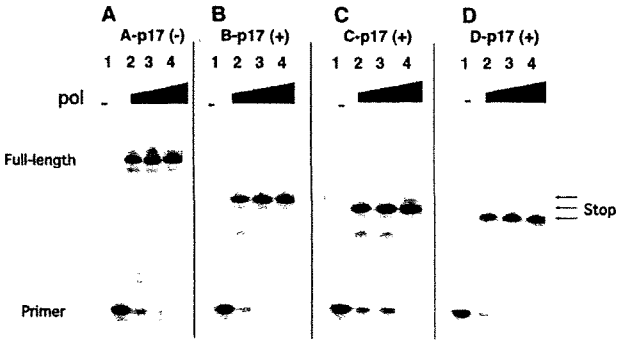

FIGURE 2. ***In vitro* DNA synthesis using Klenow fragment.** Gel electrophoresis indicating the primer extensions obtained using the 32-mer oligonucleotide templates, p32A (*A*), p32B (*B*), p32C (*C*), and p32D (*D*), which have no PhIP adduct, and a PhIP adduct on the first, second, and third G within the triple G sequence, respectively. The 3′ complementary 17-mer sequence, p17, was used as the extension primer. The final concentration of each template-primer complex was 12.5 nM. Concentrations of Klenow fragment were 0 (*lane 1*), 7.8 (*lane 2*), 23 (*lane 3*), and 78 units/ml (*lane 4*).

extension experiments using p32B, p32C, and p32D as templates were carried out (see Table 1). The length of each produced fragment was precisely determined using ladders of oligonucleotide fragments as markers (data not shown). The Klenow fragment of *E. coli* DNA polymerase I, a member of the A-family DNA polymerases, was first used in this analysis. The production of a 28-, 27-, and 26-mer from these primer extension reactions using B-p17, C-p17, and D-p17, respectively, using a template-primer complex, and lack of longer fragments indicated that the Klenow fragment stalled just before the dG-C8-PhIP adduct (Fig. 2). On the other hand, control experiments using p32A without the adduct as a template produced a 32-mer fragment (Fig. 2*A*). Similar results were obtained with *E. coli* DNA polymerase I (exo$^+$) and B-family DNA polymerases, such as the thermophilic bacterial DNA polymerases, r*Taq* and *Tth*, and human DNA polymerase α (data not shown) (supplemental Fig. S2), suggesting that stalling at the dG-C8-PhIP adduct occurs for all replicative DNA polymerases. Stalling of r*Taq* and *Tth* at the PhIP adduct was observed at 65 °C, as well as at 37 °C, indicating that this is the result of a physical hindrance of the adduct itself and not from secondary DNA structures. Moreover, there was no difference found between the stalling of *E. coli* DNA polymerase I (exo$^+$) and that of the Klenow fragment (exo$^-$). This indicates that the physical blocking of DNA polymerases at the dG-C8-PhIP adduct does not depend upon their proofreading function.

Finally, DNA synthesis analyses with human DNA polymerase δ (pol δ), a member of the B-family DNA polymerases and a truly replicative polymerase, were carried out. In the case of using p32C and p17 (C-p17) as a template-primer complex, the production of 27-mer fragments indicated the stalling of pol δ just before the PhIP adduct (Fig. 3, *lane 11*). From a control reaction using A-p17, a template-primer complex without the PhIP adduct, a full-length product of 32-mer was generated (Fig. 3, *lane 8*). In addition to these major products, minor products extended one nucleotide further (28- and 33-mer) and ladders of bands indicating degradation of primer (<17-mer) were observed (Fig. 3), corresponding with previous results reporting terminal dA transferase and exonuclease activities of pol δ (32). PCNA, an accessory protein acting as a sliding clamp for pol δ, was previously reported to promote DNA synthesis by pol δ past several template lesions, including abasic sites, 8-oxo-dG, and aminofluorene-dG (32). In the case of dG-C8-PhIP, however, PCNA was unable to promote the bypass synthesis of pol δ beyond the lesion (Fig. 3, *lane 12*). Extension reaction from the longer 22-mer primer, p22, also paused completely just before the PhIP adduct in the presence or absence of PCNA (Fig. 3, *lanes 5* and *6*). These results strongly suggest that the dG-C8-PhIP adduct on genome DNA in the living cells induces the complete block of replication forks including pol δ, PCNA, and pol α.

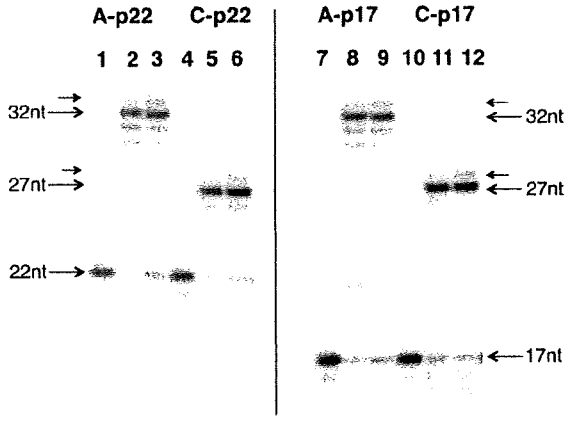

FIGURE 3. ***In vitro* DNA synthesis using pol δ in the presence or absence of PCNA.** Gel electrophoresis indicating the primer extensions obtained using the 32-mer oligonucleotide templates, p32A (*A*), and p32C (*C*), which have no PhIP adduct, and a PhIP adduct on the second G within the triple G sequence, respectively. The 3′ complementary 22- and 17-mer sequences, p22 and p17, were used as the extension primer. The final concentration of each template-primer complex was 12.5 nM. Concentrations of pol δ were 0 (*lanes 1, 4, 7,* and *10*) and 16 nM (*lanes 2, 3, 5, 6, 8, 9, 11,* and *12*). Concentrations of PCNA as a trimer were 0 (*lanes 1, 2, 4, 5, 7, 8, 10,* and *11*) and 20 nM (*lanes 3, 6, 9,* and *12*). *Large arrows* indicate the positions of primers (17- or 22-mer), full-length products (32-mer), and the products pausing just before the PhIP adduct (27-mer). *Small arrows* indicate the minor products that incorporated an additional 1 nucleotide (*nt*) to a full-length product or the pausing product.

Translesional DNA Synthesis by Y-family DNA Polymerases—Translesional DNA synthesis at the dG-C8-PhIP adduct by the Y-family DNA polymerases, pol η, pol κ, pol ι, and REV1 was next examined. Two substrates, C-p27 and C-p28, and their counterparts without a PhIP adduct, A-p27 and A-p28, were used in these experiments (Fig. 4). Substrate C-p27 was prepared by annealing the p32C template (see Table 1) to its 3′-complimentary 27-mer sequence, p27, and was used to identify the nucleotides that are inserted opposite the dG-C8-PhIP adduct (Fig. 4). Similarly, substrate C-p28 was used to analyze the extension reaction from the 3′-end of the dC bases opposite the dG-C8-PhIP adduct (Fig. 4). We found that recombinant human DNA polymerase η (pol η) could insert a dC opposite the dG-C8-PhIP adduct, although at low efficiency compared with control experiments without the PhIP adduct (Fig. 5, *A* and *B*). Extension reactions catalyzed by pol η from the 3′-end of dC opposite the adduct were barely detectable (Fig. 5*D*), although an excessive amount of pol η produced byproducts that incorporated a mismatch nucleotide, dG, dA, or dT (supplemental Fig. S4). In the case of dG, incorporation of one to three dG nucleotides was observed (supplemental Fig. S4). In control experiments without the PhIP adduct, minor products were produced that incorporated mismatch nucleotides, in addition to a major product that incorporated a dC (Fig. 5*C*).

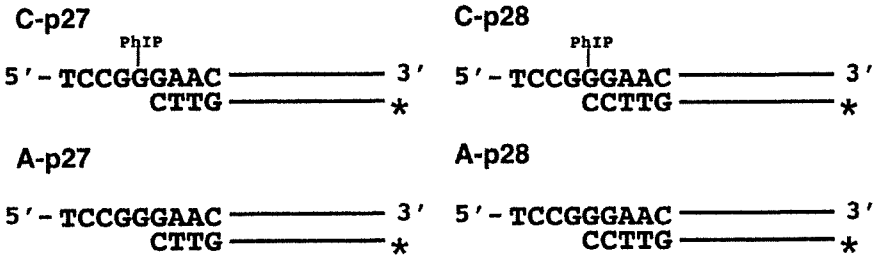

FIGURE 4. **Template-primer complexes.** Substrates C-p27 and C-p28 (series-C) have a PhIP adduct on the second dG within a GGG sequence. Substrates A-p27 and A-p28 (series-A) are control substrates without a PhIP adduct. The corresponding 3′ complimentary 27- and 28-mer sequences, p27 and p28, were used as extension primers. The template-primer complexes, C-p27 and C-p28, were used to monitor the nucleotide insertions into the site opposite dG-C8-PhIP and the extension reactions from the 3′-dC opposite dG-C8-PhIP, respectively.

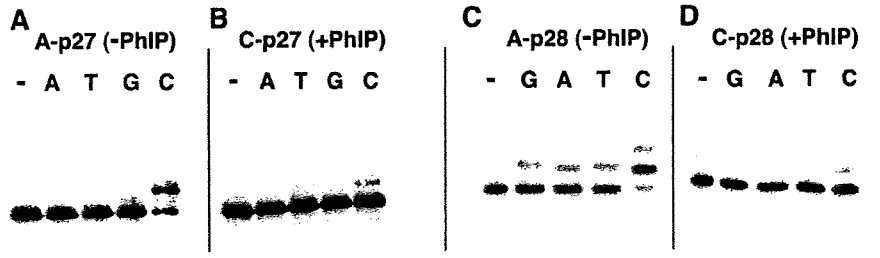

FIGURE 5. **Translesional DNA synthesis by pol η using substrates C-p27 and C-p28.** Control reactions were performed using substrates without the PhIP adduct, A-p27 (*A*) and A-p28 (*C*). An insertion reaction was performed with substrate C-p27 (*B*) and an extension reaction with substrate C-p28 (*D*). A single dNTP (G, A, T, C) was added into the reaction mixture as indicated by *G, A, T,* and *C above* each lane. The lanes indicated by − are controls without any nucleotides. Concentrations of pol η and each dNTP were 1.9 nM and 100 μM, respectively.

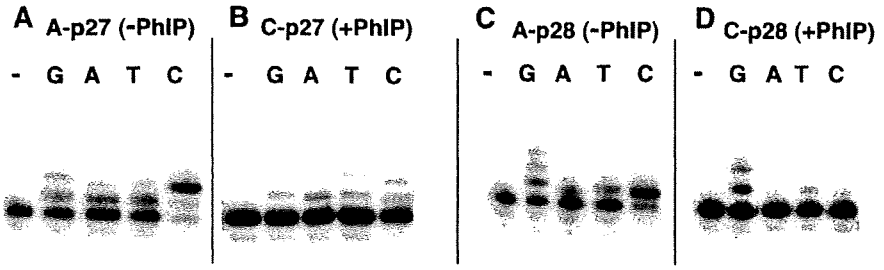

FIGURE 6. **Translesional DNA synthesis by pol κ using substrates C-p27 and C-p28.** Control reactions were performed using substrates without the PhIP adduct, A-p27 (*A*) and A-p28 (*C*). An insertion reaction was performed with substrate C-p27 (*B*) and an extension reaction with substrate C-p28 (*D*). A single dNTP (G, A, T, C) was added into the reaction mixture as indicated by *G, A, T,* and *C above* each lane. The lanes indicated by − are controls without any nucleotides. The concentrations of pol κ were 250 (*A* and *C*), 500 (*B*), and 1000 nM (*D*), respectively. The concentration of each dNTP was 100 μM.

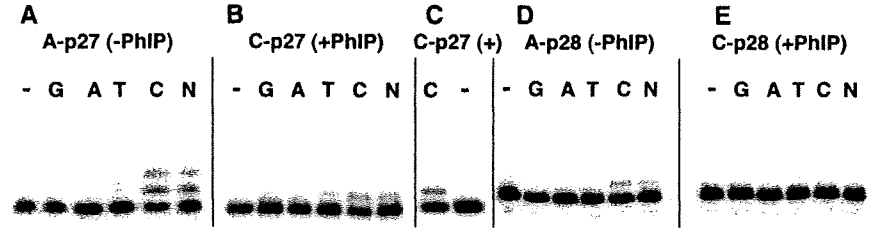

FIGURE 7. **Translesional DNA synthesis by REV1 using substrates C-p27 and C-p28.** Control reactions were performed using substrates without the PhIP adduct, A-p27 (*A*) and A-p28 (*D*). Insertion reactions were performed with substrate C-p27 (*B* and *C*) and an extension reaction with substrate C-p28 (*E*). A single dNTP (G, A, T, and C) or a mixture of each was added into the reaction mixture as indicated by *G, A, T, C,* and *N above* each lane. The lanes indicated by − are controls without any nucleotides. The concentrations of REV1 were 5.2 (*A* and *D*) and 26 nM (*B, C,* and *E*), respectively. The concentrations of each dNTP were 100 μM (*A, B, D,* and *E*) and 320 μM (*C*), respectively. The *N* mixture contained each dNTP at a concentration of 25 μM.

We next examined translesional DNA synthesis beyond the PhIP adduct using a truncated form of human DNA polymerase κ containing the N-terminal 559 amino acids. One or two dCs were inserted opposite the dG-C8-PhIP adduct by this polymerase, and misinsertions of three other nucleotides were also observed to a certain extent (Fig. 6*B*). pol κ incorporated two dCs and misincorporated dG, dA, and dT into the A-p27 substrate without the PhIP adduct at a low efficiency (Fig. 6*A*). Misincorporations of dG, dA, and dT into the A-p28 substrate without the adduct were also observed (Fig. 6*C*). In the case of the extension reaction from 3′-dC opposite the dG-PhIP adduct, pol κ also incorporated dC and misincorporated dT into the C-p28 substrate at low efficiency (Fig. 6*D*). Interestingly, one- and two-base incorporations of dG into the substrate C-p28 by pol κ dominated the incorporation of a dC (Fig. 6*D*). In the extension reaction with pol κ in the presence of all four dNTPs, fragments of 29 and 30 nucleotides were observed as major products, and a small amount of the 31-nucleotide fragment was observed (see supplemental Fig. S5, *lane 6*). Full-length products of 32 nucleotides were observed only when an excess amount of pol κ was present (data not shown). This poor extension activity of pol κ after adding two nucleotides was probably caused by the shortness (~4 nucleotides) of the 5′ region to the lesion in the template oligonucleotide. Extension with pol κ, pol η, and pol δ from the mismatched primers, where the 3′-terminal nucleotide of the p28 primer, dC, was substituted with another nucleotide, could not be observed (data not shown). REV1 inserted a dC opposite the PhIP adduct at a higher efficiency compared with pol κ and pol η (Fig. 7, *B* and *C*). REV1 was, however, unable to catalyze the extension reaction from the dC opposite the PhIP adduct in C-p28 (Fig. 7*E* and supplemental Fig. S5, *lane 5*). REV1 incorporated only dC nucleotides into A-p27 and A-p28 substrates without the adduct (Fig. 7, *A* and *D*). Neither nucleotide insertion nor extension reactions for the templates containing the PhIP adduct were detected using human pol ι (data not shown).

Kinetic Analyses of Translesional DNA Synthesis by pol κ and REV1—To evaluate translesional DNA synthesis beyond the dG-C8-PhIP adduct in further detail, additional quantitative analyses for pol κ and REV1 were performed. Insertion reactions catalyzed by pol κ for dC (Fig. 8, *B, lanes 2–5,* and *C, closed diamonds*) and dG (Fig. 8, *B, lanes 6–9,* and *C, closed triangles*) into substrate C-p28 were analyzed in the same way. Kinetic parameters for pol κ were determined using steady-state kinetic assays (Table 2). The catalytic efficiency (k_{cat}/K_m) of dC insertion into C-p28 (0.039 min^{-1} mM^{-1}) was found to be 4-fold greater than that into C-p27 (0.011 min^{-1} mM^{-1}). These results indicate that pol κ catalyzes the extension reaction from the 3′-terminal of dC opposite the dG-C8-PhIP with a higher efficiency than the insertion reaction opposite the adduct. The k_{cat}/K_m values of the dC insertion opposite the adduct were roughly 4 orders of magnitude less than those into counterparts without the adduct (see Table 2). The k_{cat}/K_m value of the dG incorporation into C-p28 was slightly higher than that of dC, and more than 8-fold higher than that of dG into C-p27 (see Table 2). This result indicates that pol κ skipped over the dG site just 5′ of dG-C8-PhIP on the template and incorporated dG opposite dC on the template strand of substrate C-p28 with a high efficiency. The k_{cat}/K_m values of the dC incorporation into D-p27 (0.19 min^{-1} mM^{-1}) were over 4-fold greater than into C-p28 (0.039 min^{-1} mM^{-1}) and over 8-fold higher than that of dG into B-p29 (0.023) (see supplemental Table S1). These data indicate that the efficiencies of the extension reaction by pol κ are the highest for template p32D containing the PhIP adduct in the third G of the triple G run, next for template p32C containing the PhIP/adduct in the second G, and lowest for template p32B containing the PhIP adduct in the first G.

Even at higher concentrations of dNTPs, extension reactions catalyzed by REV1 for substrate C-p28 could not be monitored (Table 3, Fig. 7*E*). The k_{cat}/K_m value of the dC incorporation by REV1 into substrate C-p27 was more than 2,000 times greater than that by pol k, and 1/44 of the values for counterparts with-

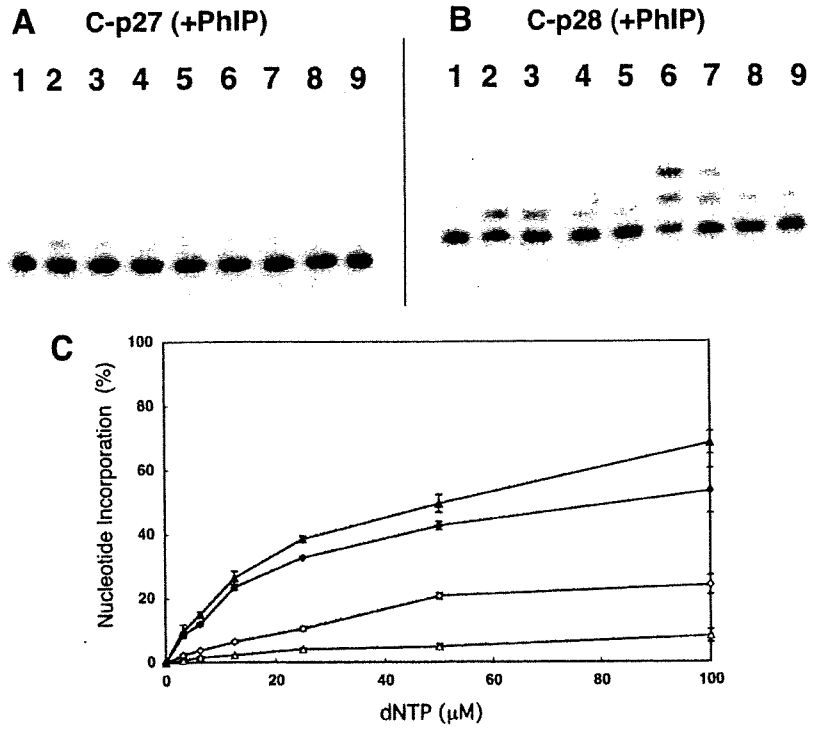

FIGURE 8. **Translesional DNA synthesis by pol κ.** Nucleotide incorporation by pol κ for substrates C-p27 (*A*) and C-p28 (*B*). Either dCTP (*lanes 2-5*) or dGTP (*lanes 6-9*) was added into the reaction mixture. *Lane 1* indicates a control without any nucleotides. The concentration of pol κ was 910 nM. The concentrations of dCTP or dGTP, respectively, were 25 (*lanes 2* and *6*), 12.5 (*lanes 3* and *7*), 6.25 (*lanes 4* and *8*), and 3.13 μM (*lanes 5* and *9*). *C*, incorporation efficiencies of dCTP and dGTP into substrate C-p27 and C-p28. Incorporations of dCTP into C-p27, dGTP into C-p27, dCTP into C-p28, and dGTP into C-p28 are indicated by *open diamonds*, *open triangles*, *closed diamonds*, and *closed triangles*, respectively. Each data point represents the mean of two separate experiments. The *error bars* represent residuals.

TABLE 2
k_{cat}/K_m values for pol κ

Substrate	K_m	k_{cat}	k_{cat}/K_m
	μM	$\times 10^{-3}$ min^{-1}	min^{-1} mM^{-1}
C-p27			
dCTP	70	0.76	0.011
dGTP	47	0.24	0.0050
C-p28			
dCTP	8.0	0.32	0.039
dGTP	11	0.48	0.042
A-p27			
dCTP	0.035	4.4	130
dGTP	0.26	1.3	5.0
A-p28			
dCTP	0.027	3.7	140
dGTP	2.1	8.8	4.1

TABLE 3
k_{cat}/K_m values for dCTP-insertion by REV1

Substrate	K_m	k_{cat}	k_{cat}/K_m
	μM	$\times 10^{-3}$ min^{-1}	min^{-1} mM^{-1}
C-p27	12	320	27
C-p28	ND[a]	ND	ND
A-p27	0.36	390	1100

[a] ND, not detectable.

out the adduct (Table 3). The k_{cat}/K_m values of the dC insertion by REV1 into three substrates, B-p28, C-p27 and D-p26, were 39, 27, and 73 min^{-1} mM^{-1}, respectively. Thus, the insertion reaction catalyzed by REV1 among the three templates was the most efficient for template p32D containing the PhIP adduct at the third G, similar to the extension reaction by pol κ.

DISCUSSION

In Vitro TLS Analysis Reconstituting PhIP-induced Mutations—HCAs are food-borne carcinogens produced when cooking meat (1, 9, 33). The most significant aspect of these molecules is that they exist normally in cooked food and are thus ubiquitous carcinogens (32). The mutagenicity and carcinogenicity of HCAs are mainly attributed to C8- and N2-dG adducts (9). Both excision repair and translesional DNA synthesis play critical roles in the mutagenesis steps induced by HCAs. However, despite the importance of HCAs as common environmental mutagens, there have been very few previous reports regarding the stalling of DNA polymerases and TLS caused by the DNA adducts they form. This is mainly because of the difficulty in preparing template DNA with introduced HCA adducts at specific sites. Choi *et al.* (34) have recently undertaken a biochemical study of TLS at adducts of the HCA 2-amino-3-methylimidazo[4,5-*f*]quinoline (IQ) using purified human polymerases. In our current study of TLS, we describe our findings for adducts of PhIP, the most abundant HCA in cooked foods (4).

A rat colon cancer model induced by PhIP shows profiles of cancer development similar to the multistep model of colon carcinogenesis in humans (35). In this rat model, *p53* and K-*ras* mutations are rarely observed, whereas mutations in *Apc* and its downstream gene *β-catenin* have been frequently observed (21, 36–38). Hence, mutations in *Apc* or *β-catenin* have been speculated to play a critical role in PhIP-induced colon carcinogenesis. Five mutations in the *Apc* gene were previously detected in four of eight PhIP-induced rat colon tumors, and all of these mutations involved a single guanine deletion in the 5′-GGGA-3′ sequence (21). This characteristic mutation induced by PhIP, 5′-GGGA-3′ to 5′-GGA-3′, was also observed in other *in vivo* mutation analyses using transgenic animals harboring introduced reporter genes, such as *lacI* (18–20). Hence, the 5′-TCCGGGAAC-3′ sequence corresponding to a mutation hot spot within the rat *Apc* gene, which we utilized to introduce the PhIP adduct and employed as the template for *in vitro* DNA synthesis analyses, could be a suitable model for revealing the molecular mechanisms associated with PhIP-induced mutations.

As discussed later, our results indicate a possible molecular mechanism for the 5′-GGGA-3′ to 5′-GGA-3′ mutation induced by PhIP.

DNA Polymerases Involved in TLS through the dG-PhIP Adduct—TLS through many DNA lesions requires the action of two different polymerases, an "inserter" and an "extender," the former to perform nucleotide insertions opposite the lesion site and the latter for subsequent extensions (39). The catalytic efficiency of the dCTP-insertion reaction opposite the dG-PhIP adduct by REV1 was found to be more than 2,000-fold greater than that by pol κ (see Tables 2 and 3). This result strongly suggests that REV1 functions *in vivo* as an inserter polymerase for TLS through the dG-PhIP adduct. This insertion step by REV1 is also error free. REV1 has been reported previously to insert dCTP opposite abasic sites and various N2-dG adducts (26, 39–41). However, our current study is the first to show that REV1 inserts dCTP opposite a large size C8-dG adduct. We used a shorter (C-terminal deleted) form of pol κ in our current experiments and an intact pol κ may be more effective for this insertion reaction. As for pol η, a detailed kinetic analysis was not performed. Hence, the possibility cannot be excluded that pol κ and pol η also function as inserter polymerases.

In addition to the Y-family DNA polymerases, DNA polymerase ζ (pol ζ), belonging to the B-family DNA polymerases, is considered to be involved in TLS through various lesions as an extender DNA polymerase (39, 42, 43). We have not carried out a primer extension assay with pol ζ and thus the possibility cannot be completely excluded by our current data that pol ζ functions *in vivo* as an extender polymerase for TLS through the dG-PhIP adduct. In our present study, we provide evidence that pol κ can extend from dC opposite the dG-C8-PhIP adduct *in vitro*. It is, therefore, possible that pol κ, at least partially, functions as an extender polymerase *in vivo* for TLS through the dG-PhIP adduct. Further study about cooperation between two or more DNA polymerases, including pol ζ, is necessary to verify which DNA polymerases are involved in the bypass synthesis through the PhIP lesion.

The catalytic efficiency of pol κ for a dGTP insertion into substrate C-p28 was a little higher than that for dCTP insertions (see Table 2 and Fig. 6*D*). The former generates a single guanine deletion, and the latter is an error-free extension. Consequently, our data suggest that the extension reaction with pol κ from the nucleotide opposite the dG-C8-PhIP adduct causes frequent single-guanine deletions from the GGG stretch. It has been reported that one characteristic feature of pol κ homologs, from bacteria to humans, is their propensity to generate single-base deletions (44–47). The crystal structure of Dpo4, a thermophilic archaea homolog of pol κ, in ternary complexes with DNA and an incoming nucleotide supports the model that a single base deletion by pol κ is generated through a misaligned intermediate complex where the template dG forms an extrahelical looped out structure and the incoming dGTP skips this extrahelical base and pairs with the next template base dC (48) (see supplemental Fig. S6). It is reasonable to speculate therefore that, in the case of TLS through dG-C8-PhIP, mammalian pol κ generates the single guanine deletion via a similar intermediate where the PhIP-adducted dG is looped out and template-primer slippage occurs. However, further analyses for determining whether the one-base skipping of pol κ beyond the lesion observed by us is dependent on the nucleotide placed 5′ to the lesion or not, are necessary to clarify the detailed molecular mechanism underlying one base skipping of pol κ.

Molecular Mechanisms Underlying Mutation Induction by PhIP—We have demonstrated herein by *in vitro* DNA synthesis analyses using oligonucleotide templates containing dG-PhIP that: 1) replicative DNA polymerases stall at the PhIP adduct and cannot perform translesional DNA synthesis beyond this point; 2) REV1 inserts a dC opposite the dG-PhIP with a much higher efficiency than other TLS polymerases, including pol κ and pol η; and 3) pol κ has a potential ability to catalyze an extension reaction from the 5′-dC opposite the adduct and often skips over one dG in the template during this extension step. A working model for the induction of mutations at the PhIP adducts based on the results shown in the present study is illustrated in supplemental Fig. S6. This model could be adopted for other sequences containing a G repeat stretch longer than GGG.

REFERENCES

1. Nagao, M. (2000) in *Food Borne Carcinogens: Heterocyclic Amines* (Nagao, M., and Sugimura, T., eds) pp. 163–196, John Wiley & Sons Ltd., Chichester, UK
2. Schut, H. A., and Snyderwine, E. G. (1999) *Carcinogenesis* **20,** 353–368
3. Felton, J. S., Knize, M. G., Shen, N. H., Lewis, P. R., Andresen, B. D., Happe, J., and Hatch, F. T. (1986) *Carcinogenesis* **7,** 1081–1086
4. Felton, J. S., Jagerstad, M., Knize, M. G., Skog, K., and Wakabayashi, K. (2000) in *Food Borne Carcinogens: Heterocyclic Amines* (Nagao, M., and Sugimura, T., eds) pp. 31–71, John Wiley & Sons Ltd., Chichester, UK
5. Holme, J. A., Wallin, H., Brunborg, G., Søderlund, E. J., Hongslo, J. K., and Alexander, J. (1989) *Carcinogenesis* **10,** 1389–1396
6. Felton, J. S., and Knize, M. G. (1991) *Mutat. Res.* **259,** 205–217
7. Ohgaki, H., Takayama, S., and Sugimura, T. (1991) *Mutat. Res.* **259,** 399–410
8. Ito, N., Hasegawa, R., Sano, M., Tamano, S., Esumi, H., Takayama, S., and Sugimura, T. (1991) *Carcinogenesis* **12,** 1503–1506
9. Sugimura, T., Wakabayashi, K., Nakagama, H., and Nagao, M. (2004) *Cancer Sci.* **95,** 290–299
10. Imaida, K., Hagiwara, A., Yada, H., Masui, T., Hasegawa, R., Hirose, M., Sugimura, T., Ito, N., and Shirai, T. (1996) *Jpn. J. Cancer Res.* **87,** 1116–1120
11. Frandsen, H., Grivas, S., Andersson, R., Dragsted, L., and Larsen, J. C. (1992) *Carcinogenesis* **13,** 629–635
12. Lin, D., Kaderlik, K. R., Turesky, R. J., Miller, D. W., Lay, J. O., Jr., and Kadlubar, F. F. (1992) *Chem. Res. Toxicol.* **5,** 691–697
13. Snyderwine, E. G., Davis, C. D., Nouso, K., Roller, P. P., and Schut, H. A. (1993) *Carcinogenesis* **14,** 1389–1395
14. Schut, H. A., and Herzog, C. R. (1992) *Cancer Lett.* **67,** 117–124
15. Endo, H., Schut, H. A., and Snyderwine, E. G. (1994) *Cancer Res.* **54,** 3745–3751
16. Morgenthaler, P. M., and Holzhäuser, D. (1995) *Carcinogenesis* **16,** 713–718
17. Yadollahi-Farsani, M., Gooderham, N. J., Davies, D. S., and Boobis, A. R. (1996) *Carcinogenesis* **17,** 617–624
18. Okonogi, H., Stuart, G. R., Okochi, E., Ushijima, T., Sugimura, T., Glickman, B. W., and Nagao, M. (1997) *Mutat. Res.* **395,** 93–99
19. Lynch, A. M., Gooderham, N. J., Davies, D. S., and Boobis, A. R. (1998) *Mutagenesis* **13,** 601–605
20. Okochi, E., Watanabe, N., Shimada, Y., Takahashi, S., Wakazono, K., Shirai, T., Sugimura, T., Nagao, M., and Ushijima, T. (1999) *Carcinogenesis* **20,** 1933–1988
21. Kakiuchi, H., Watanabe, M., Ushijima, T., Toyota, M., Imai, K., Weisburger, J. H., Sugimura, T., and Nagao, M. (1995) *Proc. Natl. Acad. Sci.*

U.S.A. **92,** 910–914
22. Takamura-Enya, T., Ishikawa, S., Mochizuki, M., and Wakabayashi, K. (2006) *Chem. Res. Toxicol.* **19,** 770–778
23. Masuda, Y., Suzuki, M., Piao J., Gu, Y., Tsurimoto, T., and Kamiya, K. (2007) *Nucleic Acids Res.* **35,** 6904–6916
24. Masutani, C., Kusumoto, R., Iwai, S., and Hanaoka, F. (2000) *EMBO J.* **19,** 3100–3109
25. Niimi, N., Sassa, A., Katafuchi, A., Grúz, P., Fujimoto, H., Bonala, R. R., Johnson, F., Ohta, T., and Nohmi, T. (2009) *Biochemistry* **48,** 4239–10234246
26. Masuda, Y., and Kamiya, K. (2002) *FEBS Lett.* **520,** 88–92
27. Masuda, Y., Ohmae, M., Masuda, K., and Kamiya, K. (2003) *J. Biol. Chem.* **278,** 12356–12360
28. Sambrook, J., Fritsch, E. F., and Maniatis, T. (1989) *Molecular Cloning: A Laboratory Manual,* 2nd Ed., Cold Spring Harbor Laboratory, Cold Spring Harbor, NY
29. Fukuda, H., and Ohtsubo, E. (1997) *Genes Cells* **2,** 735–751
30. Fukuda, H., Katahira, M., Tsuchiya, N., Enokizono, Y., Sugimura, T., Nagao, M., and Nakagama, H. (2002) *Proc. Natl. Acad. Sci. U.S.A.* **99,** 12685–12690
31. Sugiyama, H., and Saito, I. (1996) *J. Am. Chem. Soc.* **118,** 7063–7068
32. Mozzherin, D. J., Shibutani, S., Tan, C. K., Downey, K. M., and Fisher, P. A. (1997) *Proc. Natl. Acad. Sci. U.S.A.* **94,** 6126–6231
33. Sugimura, T., and Adamson, R. H. (2000) in *Food Borne Carcinogens: Heterocyclic Amines* (Nagao, M., and Sugimura, T., eds) pp. 1–4, John Wiley & Sons Ltd., Chichester, UK
34. Choi, J. Y., Stover, J. S., Angel, K. C., Chowdhury, G., Rizzo, C. J., and Guengerich, F. P. (2006) *J. Biol. Chem.* **281,** 25297–25306
35. Nakagama, H., Ochiai, M., Ubagai, T., Tajima, R., Fujiwara, K., Sugimura, T., and Nagao, M. (2002) *Mutat. Res.* **506–507,** 137–144
36. Nagao, M. (1999) *Mutat. Res.* **431,** 3–12
37. Nagao, M., Ushijima, T., Toyota, M., Inoue, R., and Sugimura, T. (1997) *Mutat. Res.* **376,** 161–167
38. Dashwood, R. H., Suzui, M., Nakagama, H., Sugimura, T., and Nagao, M. (1998) *Cancer Res.* **58,** 1127–1129
39. Prakash, S., Johnson, R. E., and Prakash, L. (2005) *Annu. Rev. Biochem.* **74,** 317–353
40. Nelson, J. R., Lawrence, C. W., and Hinkle, D. C. (1996) *Nature* **382,** 729–731
41. Haracska, L., Prakash, S., and Prakash, L. (2002) *J. Biol. Chem.* **277,** 15546–15551
42. Johnson, R. E., Washington, M. T., Haracska, L., Prakash, S., and Prakash, L. (2000) *Nature* **406,** 1015–1019
43. Haracska, L., Unk, I., Johnson, R. E., Johansson, E., Burgers, P. M., Prakash, S., and Prakash, L. (2001) *Genes Dev.* **15,** 945–954
44. Kim, S. R., Maenhaut-Michel, G., Yamada, M., Yamamoto, Y., Matsui, K., Sofuni, T., Nohmi, T., and Ohmori, H. (1997) *Proc. Natl. Acad. Sci. U.S.A.* **94,** 13792–13797
45. Kobayashi, S., Valentine, M. R., Pham, P., O'Donnell, M., and Goodman, M. F. (2002) *J. Biol. Chem.* **277,** 34198–34207
46. Ogi, T., Kato, T., Jr., Kato, T., and Ohmori, H. (1999) *Genes Cells* **4,** 607–618
47. Ohashi, E., Bebenek, K., Matsuda, T., Feaver, W. J., Gerlach, V. L., Friedberg, E. C., Ohmori, H., and Kunkel, T. A. (2000) *J. Biol. Chem.* **275,** 39678–39684
48. Ling, H., Boudsocq, F., Woodgate, R., and Yang, W. (2001) *Cell* **107,** 91–102

Published online 29 April 2009

Nucleic Acids Research, 2009, Vol. 37, No. 12 ***3959–3968***
doi:10.1093/nar/gkp262

The ATR-Chk1 pathway plays a role in the generation of centrosome aberrations induced by Rad51C dysfunction

Mari Katsura[1,2], Takanori Tsuruga[2], Osamu Date[2], Takashi Yoshihara[2], Mari Ishida[2], Yoshitaka Tomoda[1], Miyuki Okajima[1], Motoki Takaku[3], Hitoshi Kurumizaka[3], Aiko Kinomura[2], Hiromu K. Mishima[4] and Kiyoshi Miyagawa[1,2,*]

[1]Laboratory of Molecular Radiology, Center for Disease Biology and Integrative Medicine, Graduate School of Medicine, The University of Tokyo, 7-3-1 Hongo, Bunkyo-ku, Tokyo 113-0033, [2]Department of Human Genetics, Research Institute for Radiation Biology and Medicine, Hiroshima University, 1-2-3 Kasumi, Minami-ku, Hiroshima 734-8553, [3]Laboratory of Structural Biology, Graduate School of Advanced Science and Engineering, Waseda University, 2-2 Wakamatsu-cho, Shinjuku-ku, Tokyo 162-8480 and [4]Department of Ophthalmology, Graduate School of Medical Sciences, Hiroshima University, 1-2-3 Kasumi, Minami-ku, Hiroshima 734-8553, Japan

Received September 4, 2008; Revised March 6, 2009; Accepted April 8, 2009

ABSTRACT

Rad51C is a central component of two complexes formed by five Rad51 paralogs in vertebrates. These complexes are involved in repairing DNA double-strand breaks through homologous recombination. Despite accumulating evidence suggesting that the paralogs may prevent aneuploidy by controlling centrosome integrity, Rad51C's role in maintaining chromosome stability remains unclear. Here we demonstrate that Rad51C deficiency leads to both centrosome aberrations in an ATR-Chk1-dependent manner and increased aneuploidy in human cells. While it was reported that Rad51C deficiency did not cause centrosome aberrations in interphase in hamster cells, such aberrations were observed in interphase in HCT116 cells with Rad51C dysfunction. Caffeine treatment and down-regulation of ATR, but not that of ATM, reduced the frequency of centrosome aberrations in the mutant cells. Silencing of Rad51C by RNA interference in HT1080 cells resulted in similar aberrations. Treatment with a Chk1 inhibitor and silencing of Chk1 also reduced the frequency in HCT116 mutants. Accumulation of Chk1 at the centrosome and nuclear foci of γH2AX were increased in the mutants. Moreover, the mutant cells had a higher frequency of aneuploidy. These findings indicate that the ATR-Chk1 pathway plays a role in increased centrosome aberrations induced by Rad51C dysfunction.

INTRODUCTION

Homologous recombination, along with nonhomologous end-joining, plays a major role in the repair of DNA double-stranded breaks (DSBs) (1). Rad51 is a key player in homologous recombination by exerting homologous pairing and strand exchange activities. Rad51 paralogs are assumed to be involved in the early stages of homologous recombination by assisting Rad51 function (2). Five members of the Rad51 paralog family constitute two protein complexes: Rad51B-Rad51C-Rad51D-XRCC2 (BCDX2) and Rad51C-XRCC3 (3,4). Thus, Rad51C is a central component among five members in vertebrates.

The centrosome serves as the microtubule-organizing center, ensuring correct chromosome segregation to prevent aneuploidy (5). Accumulating evidence suggests that centrosome dysfunction, typically represented by abnormal numbers of centrosomes, is involved in human diseases, particularly in cancers (6). More than 100 proteins have been reported to be localized in the centrosome (7). Deletion of these proteins often leads to centrosome aberrations.

Mutations of XRCC2, XRCC3, Rad51B and Rad51D were shown to increase centrosome fragmentation and aneuploidy (8–10). Despite these observations, the role of Rad51C in the maintenance of centrosome integrity and chromosome stability remains unclear. Initially, Rad51C-deficient Chinese hamster ovary (CHO) cells, CL-V4B, were shown to exhibit no increase in centrosome aberrations (11). A recent study, however, demonstrated that centrosome numbers were increased only in mitosis and not in interphase in CL-V4B cells (12).

*To whom correspondence should be addressed. Tel: +81 358413503; Fax: +81 358413013; Email: miyag-tky@umin.ac.jp

Moreover, although increased numbers of centrosomes are assumed to generate aneuploidy, no studies using mammalian cells have demonstrated that Rad51C deficiency leads to increased aneuploidy.

The mechanisms underlying centrosome aberrations observed in cells with a defect in homologous recombination are controversial. In chicken DT40 cells with a conditional mutation of Rad51, the ATM-dependent checkpoint pathway was proposed to be responsible for centrosome amplification at the G2 phase (13). However, the results of a study using CHO cells with the dominant-negative Rad51 protein argued against this result (14). The hereditary breast cancer susceptibility protein BRCA1 is also involved in homologous recombination. Recent evidence suggests that HMMR, encoding the hyaluronan-mediated motility receptor, is a substrate of BRCA1-BARD1 E3 ubiquitin ligase activity and plays a role in centrosomal function (15).

Supernumerary centrosomes induced by ionizing radiation were shown to be caused by the Chk1-mediated pathway, indicating that the DNA damage response signal is involved in centrosome amplification (16). Treatment with caffeine, an inhibitor of ATM and ATR kinases, reduced centrosome amplification induced by ionizing radiation, suggesting that either or both kinases may be involved in centrosome amplification. However, caffeine treatment in ATM- or ATR-deficient cells also reduced centrosome amplification. Thus, the roles of ATM and ATR in promoting centrosome amplification induced by ionizing radiation appear to be complementary.

To investigate Rad51C's role in the maintenance of chromosome stability, we knocked out the gene in the human colon cancer cell line HCT116. We also silenced the gene by RNA interference in the human fibrosarcoma cell line HT1080. Supernumerary centrosomes in these cells with Rad51C dysfunction were increased at both interphase and metaphase in an ATR-Chk1-dependent manner. Consistent with this observation, aneuploidy was increased in HCT116 cells with Rad51C dysfunction. Our observations suggest that the ATR-Chk1 pathway plays a role in increased centrosome aberrations induced by Rad51C dysfunction in human cancer cells.

MATERIALS AND METHODS

Cell culture

HCT116 cells were cultured in McCoy's 5A medium supplemented with 10% fetal bovine serum (FBS). HT1080 cells were cultured in the minimum essential medium Eagle (MEM) supplemented with 10% FBS. These cells were obtained from the American Type Culture Collection. 2-Morpholin-4-yl-6-thianthren-1-yl-pyran-4-one (KU55933) and 7-hydroxystaurosporine (UCN-01) were purchased from Merck Calbiochem.

Generation of Rad51C mutant cells

The 8-kb left arm and 1.5-kb right arm of the *RAD51C* genomic fragments were isolated from the EMBL3 SP6/T7 human genomic library (Clontech) and inserted into pBluescript SK for neomycin and blasticidin selection. The shorter genomic fragment was isolated from the genomic DNA of HCT116 by PCR amplification for puromycin selection. The 2.4-kb left arm was amplified using primers 5′-TTTGGCTGCTCCGGGGTTA-3′ and 5′-CAGAGTTTCTAAGGCTTCTGC-3′. The 1.5-kb right arm was amplified using primers 5′-CTCGAGTGGAGTGCCCTTAAT-3′ and 5′-CTCGAGTCAACAGAAAGATGAC-3′. Promoterless neomycin-, blasticidin- and puromycin-resistant genes were inserted into the Dra I site in exon 2. Gene targeting in HCT116 was carried out as previously described (17).

Complementation experiments

The *RAD51C* cDNA was amplified from normal human cDNA using primers 5′-TTTGGCTGCTCCGGGGTTA-3′ and 5′-CATTCATGCCATAGTGTG-3′, and cloned into pCR2.1 (Invitrogen) by the TA cloning method. After the sequence was confirmed, the cDNA was inserted into an expression vector under the control of the MSV enhancer and the MMTV promoter. The generation of the XRCC3 expression vector has been described earlier (18).

Sensitivity to DNA-damaging agents

After 1×10^3 cells were cultured in a 60 mm dish for 24 h, they were exposed to mitomycin C (MMC) (Kyowa Hakko Kogyo) for 10 min, hydroxyurea (HU) (Sigma-Aldrich) for 24 h or γ-ray irradiation. They were further cultured for 9 days, and the colonies were counted.

Sister chromatid exchange (SCE) and gene targeting frequency

SCEs were analyzed essentially as previously described (17). Cells were cultured in 16 μM 5-bromodeoxyuridine (BrdU) for 36 h (wild type), 42 h (*RAD51C*$^{+/-/-/-}$) or 41 h (*RAD51C*$^{+/-/-/-}$ + cDNA), and pulsed with 0.1 μg/ml colcemid for the last 1 h. To examine the effect of MMC, cells were incubated in the presence of 0.8 μg/ml MMC for 8 h before harvest. Harvested cells were treated with 75 mM KCl:1% sodium citrate (4:1) for 20 min and fixed with methanol:acetic acid (3:1). Cells were fixed on slides and incubated with 12.8 μg/ml Hoechst 33258 for 20 min. The slides were irradiated with ultraviolet for 1 h at 60°C and stained with Giemsa solution. Gene targeting frequencies at the *RAD54B* locus were examined as previously described (17).

Antibodies

Anti-ATM (5C2), ATR (N-19), Chk1 (G-4 and DCS-310) and Cdk2 (M2) antibodies were from Santa Cruz Biotechnology. Anti-γ-tubulin (T3559 and T6557) and β-actin (A1978) antibodies were from Sigma-Aldrich. The anti-XRCC3 antibody (NB100-165) was from Novus Biologicals. Anti-phospho-H2AX Ser 139 (07-164) and Chk2 (05-649) antibodies were from Upstate Biotechnology. The anti-Chk2 antibody (DCS-273) was from Medical & Biological Laboratories. The anti-Rad51B antibody was obtained from rabbits immunized with the recombinant Rad51B protein (19). The anti-Rad51C antibody (ab3669) was from Abcam.

Immunofluorescence

Cells grown on coverslips were fixed for 10 min in 4% paraformaldehyde. Then, they were permeabilized with 0.5% Triton X-100 and 0.1% SDS/PBS for 5 min. Cells were blocked with 10% horse serum at 4°C for 30 min and incubated with primary antibodies at 37°C for 1 h and with secondary antibodies for 30 min. Finally, cells were counterstained with 4′,6′-diamidino-2-phenylindole (DAPI) and mounted. Slides were analyzed using Olympus BX51-DP70, Carl Zeiss AxioImagerZ1/Apotome and Nikon Confocal Laser Microscope system A1.

Fluorescence *in situ* hybridization analysis

Chromosome-specific centromeric probes were obtained from Vysis. DNA in cells was denatured in 70% formamide/2× SSC at 73°C for 5 min. Hybridization was performed in a CEP hybridization buffer (Vysis) at 42°C for 1 h. Slides were washed in 0.4× SSC/0.3% NP40 at 73°C for 2 min and in 2× SSC/0.1% NP40 at room temperature for 1 min. Cellular DNA was stained with DAPI.

RNA interference

siCONTROL, Rad51C siGENOME set of 4, ATM SMARTpool, ATR SMARTpool, Chk1 SMARTpool and Chk2 SMARTpool small interference RNAs (siRNAs) were purchased from Dharmacon. Cells were transfected with 100 nM siRNA and Dharmafect4 (Dharmacon) according to the manufacturer's instructions. Cells were harvested at 72 h post-transfection.

Cell-cycle analysis

Cells treated with siRNAs were harvested 72 h after transfection. EPICS XL (Beckman Coulter) was used for cell-cycle analysis.

Kinase assay

Cells were dissolved into a lysis buffer (50 mM Tris–HCl pH 7.5, 150 mM NaCl, 1% Nonidet P40, 10% glycerol and 2 mM EDTA) containing phosphatase inhibitors (50 nM cantharidin, 5 nM microcystin and 25 mM bromotetramisole oxalate), 2 mg/ml aprotinin and 0.5 mM PMSF for 15 min on ice and lysed by sonication. After centrifugation (12 000 rpm, 5 min), the supernatant was collected and precleared by incubation with normal IgG for 1 h and Protein G for 30 min. Precleared lysate was incubated with anti-Chk1 or anti-Chk2 antibody for 1 h. After incubation with Protein G, immunoprecipitates were washed three times each with the lysis buffer and 25 mM Hepes. The washed precipitate was incubated in a kinase reaction buffer (25 mM Hepes pH 7.4, 15 mM $MgCl_2$, 80 mM EGTA and 1 mM DTT) with 0.1 mM ATP, 3 μCi[γ-^{32}P]ATP and 10 μg glutathione *S*-transferase (GST)-Cdc25C (200–256) at 30°C for 30 min. The reaction was stopped by the addition of the sample buffer and subjected to SDS-PAGE. GST-Cdc25C (200–256) was prepared as previously described (20).

RESULTS

Rad51C is involved in homologous recombination in human cells

To investigate the role of Rad51C in human cells, the gene was sequentially knocked out in HCT116 cells (Figure 1A). In accordance with the finding that *RAD51C* was frequently amplified in human cancer cells, Southern blot analysis demonstrated that this cell line harbors four alleles of the gene (Figure 1B) (21,22). Two independent *RAD51C*$^{+/-/-/-}$ cell lines (#1 and #2) were isolated. The levels of Rad51C expression in proportion to targeting events were confirmed by northern and western blot analyses (Figure 1C and D). These cells were used in function analysis as Rad51C mutant cells because clear phenotypes indicating defective homologous recombination in comparison with wild-type HCT116 cells were observed. Complementation experiments were performed using cells transfected with the exogenous Rad51C expression vector.

The mean of the frequency of SCE induced by MMC per cell was 5.8 in the Rad51C mutant cells, a value that was significantly lower than 8.3, the mean value for wild-type cells (Table 1). The SCE frequency increased to a level comparable to that of the wild-type cells in cells transfected with the Rad51C expression vector. Gene targeting frequency was examined at the *RAD54B* locus, because it was assumed that Rad54B is not functionally related to Rad51C (17). The frequency in the Rad51C mutant cells was 1.16%, which was significantly lower than 12.0%, the wild-type value. These results indicate that Rad51C plays a role in homologous recombination, a finding that is in accord with the observations in DT40, CHO and HeLa cells (11,12,23,24).

Homologous recombination is required for the repair of DSBs induced by DNA-damaging agents. The Rad51C mutant cells were hypersensitive to ionizing radiation, MMC and HU, which was complemented by the exogenous expression of the gene, indicating that Rad51C plays a role in DSB repair (Figure 2A–C). A defect in homologous recombination leads to an increase in chromosome aberrations such as gaps and breaks. Giemsa staining using a metaphase spread revealed that both chromosome- and chromatid-type aberrations were increased in Rad51C mutant cells, indicating that spontaneously arising DSBs were not properly repaired (Table 2). These observations suggest that Rad51C plays a role in the repair of DSB through homologous recombination in human cells.

Rad51C dysfunction leads to increased centrosome aberrations

Since Rad51C's role in maintaining centrosome integrity has been controversial (11,12), we examined centrosome aberrations by immunostaining γ-tubulin. Cells with more than two centrosomes are observed more frequently in two independent Rad51C mutant clones than in wild-type cells (Figure 3A). The frequency of aberrant numbers of interphase centrosomes (more than two) was 7.0% in wild-type cells, whereas it was 28.0% (#1) and 30.3% (#2) in the Rad51C mutant cells. *RAD51C* cDNA expression

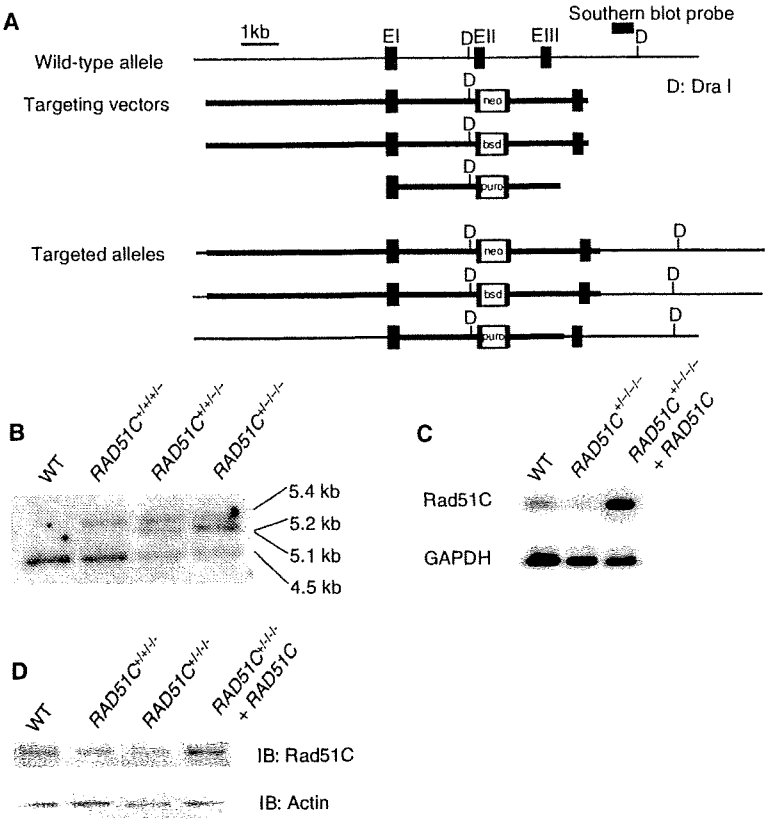

Figure 1. Generation of Rad51C mutant cells by gene targeting. (**A**) Strategy for gene targeting at the *RAD51C* locus. The targeting vectors, restriction sites and the position of the probe used for the Southern blot analysis are shown. (**B**) Southern blot analysis of DNA digested with Dra I. The size of the wild-type allele is 4.5 kb. Insertion of drug-resistance genes changes the size to 5.1, 5.2 and 5.4 kb. (**C**) Northern blot analysis of polyadenylated RNAs hybridized with the full-length *RAD51C* cDNA. (**D**) Western blot analysis. The Rad51C protein was immunoprecipitated with the rabbit polyclonal antibody and visualized by western blot analysis using the mouse monoclonal antibody.

Table 1. Sister chromatid exchanges and targeting frequency

Cell line	SCEs per cell[a]		Targeted integration[b]
	Spontaneous	MMC-induced	*RAD54B-hygro*
RAD51C$^{+/+/+/+}$	4.2 ± 0.2	8.3 ± 0.4	12.0% (13/108)
RAD51C$^{+/-/-/-}$	4.3 ± 0.3	5.8 ± 0.3[c]	1.16% (1/86)[d]
RAD51C$^{+/-/-/-}$ + cDNA	5.0 ± 0.2	8.2 ± 0.4	N.D.[e]

[a]Number of SCEs per cells represents the mean ± SEM from 100 mitotic cells.
[b]The frequency of targeted integration is shown as a percentage of the targeted clones relative to the total number of hygromycin resistant clones; the numbers of clones are given in parentheses.
[c]$P < 1.0 \times 10^{-4}$, based on Mann–Whitney U-tests, comparing wild-type cells with *RAD51C*$^{+/-/-/-}$ cells.
[d]$P = 0.0025$, based on Fisher's exact tests, comparing wild-type cells with *RAD51C*$^{+/-/-/-}$ cells.
[e]N.D., not determined.

in the mutant cells reduced the frequency to 16.3% (#2). In mitosis, the frequency was 8.0% in wild-type cells, and 24.0% (#1) and 32.8% (#2) in the mutant cells. cDNA expression in the mutant cells reduced the frequency to 21.5% (#2). Thus, unlike CHO cells with Rad51C mutation, in which centrosome aberrations were observed only at mitosis, the corresponding HCT116 cells demonstrated centrosome aberrations at both interphase and mitosis.

To confirm that a reduction in Rad51C levels leads to centrosome aberrations in other human cells, we silenced the gene in HT1080 cells by RNA interference. Western blot analysis showed that Rad51C expression was not altered in wild-type HT1080 cells and was reduced in the cells transfected with Rad51C siRNA (Figure 3B). The frequency of aberrant numbers of interphase centrosomes was 4.6% in cells transfected with control siRNA, whereas it was 9.1% in cells transfected with Rad51C siRNA (Figure 3C). Thus, supernumerary centrosomes were also increased in HT1080 cells with Rad51C dysfunction.

Rad51C affects XRCC3 levels

Since Rad51C is a central component of protein complexes formed by Rad51 paralogs, we investigated the effect of Rad51C dysfunction on the BCDX2 and Rad51C-XRCC3 complexes by measuring levels of

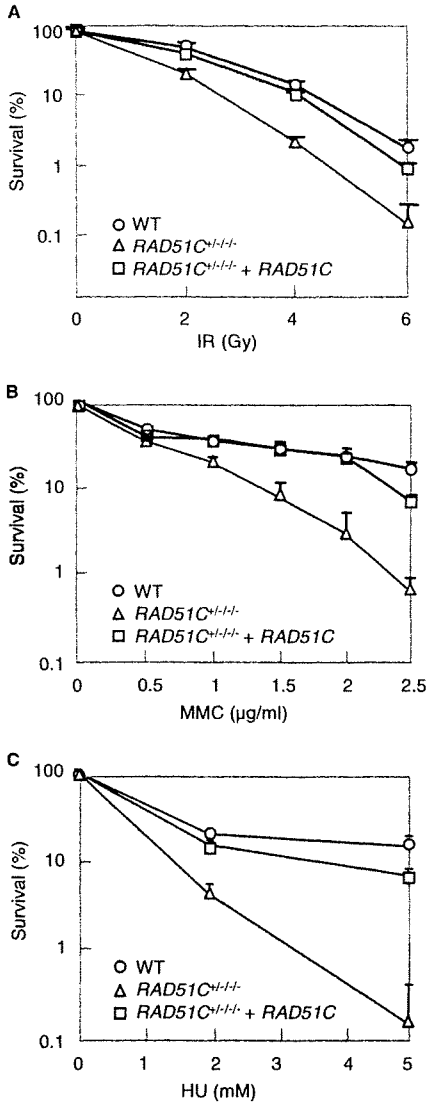

Figure 2. Sensitivity to DNA-damaging agents. (**A**) Sensitivity to ionizing radiation. (**B**) Sensitivity to MMC. (**C**) Sensitivity to HU. In (A), (B) and (C), the results represent the means ± SD of three experiments.

Table 2. Spontaneous chromosomal aberrations

Cell line	Chromatid type	Chromosome type	Abnormal cells
RAD51C$^{+/+}$	2	3	3
RAD51C$^{+/-}$	12	7	17
RAD51C$^{+/-}$ + cDNA	4	4	7

A total of 100 cells were scored for each cell line.

Rad51B and XRCC3. Western blot analysis revealed that XRCC3 levels but not Rad51B levels were reduced in the mutant cells (Figure 4A). The previous report that XRCC3 was destabilized in Rad51C-deficient human

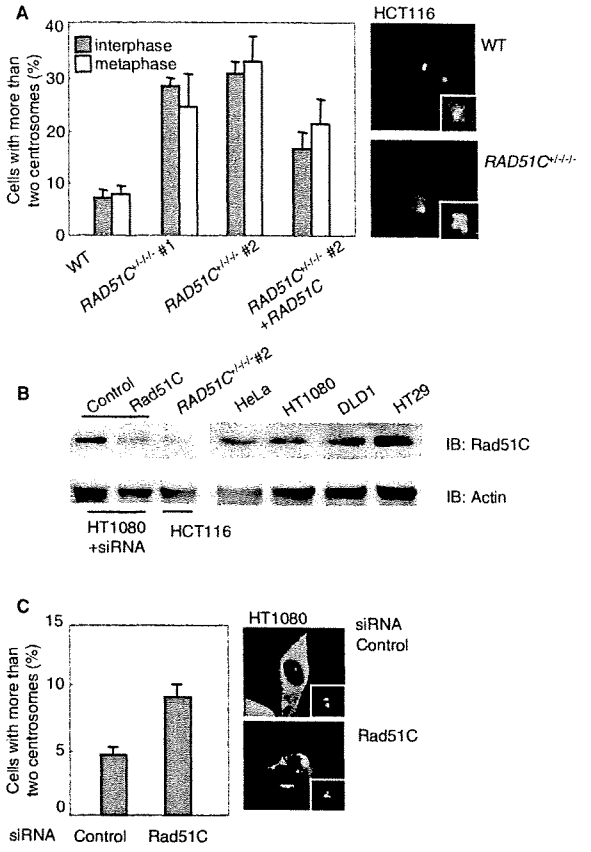

Figure 3. Centrosome aberrations. (**A**) Centrosome aberrations in HCT116 cells. For each clone at interface and metaphase, 100 cells and 50 cells, respectively, stained with the anti-γ-tubulin antibody by immunofluorescence were counted. (**B**) Western blot analysis showing the expression of Rad51C in HT1080 cells treated with either control or Rad51C siRNA. Rad51C levels in human cells are also shown as controls. (**C**) Centrosome aberrations in HT1080 cells. Cells were treated with either control or Rad51C siRNA and stained with the anti-γ-tubulin antibody. For each siRNA treatment at interface, 100 cells were counted. In (A) and (C), the results represent the means ± SEM of three independent experiments.

cells is in accord with this finding (24). Next, we investigated the effect of reduced XRCC3 levels on centrosome aberrations by expressing the *XRCC3* cDNA in the Rad51C mutant cells (Figure 4B and C). The frequency of centrosome aberrations was not changed by stable expression of XRCC3. Thus, centrosome aberrations induced by Rad51C dysfunction are unlikely to result from the destabilization of other Rad51 paralogs.

ATR is involved in promoting centrosome aberrations

We next examined the roles of ATM and ATR in centrosome aberrations in Rad51C mutant cells by a treatment with 2 mM caffeine (Figure 5A). FACS analysis confirmed that caffeine treatment at this concentration did not affect cell-cycle progression (data not shown). This treatment reduced the frequency of centrosome aberrations in the

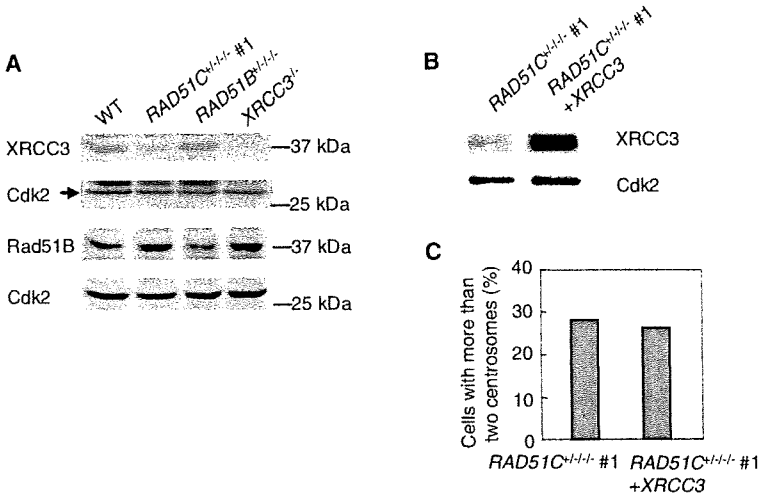

Figure 4. Effect of Rad51C dysfunction on levels of other Rad51 paralogs. (**A**) Expression of XRCC3 and Rad51B in Rad51C mutant cells. (**B**) Exogenous expression of XRCC3 in the mutant cells. (**C**) Effect of complementation of XRCC3 on centrosome aberrations in the mutant cells. A total of 200 cells were counted.

mutant from 29.0% to 15.8% ($P < 0.01$, paired t-test), indicating that ATM and/or ATR may be involved in the generation of supernumerary centrosomes.

ATM's effect on the centrosomes was examined by treatment with the ATM-specific inhibitor, KU55933 (Figure 5B). This treatment did not change the frequency of supernumerary centrosomes, indicating that ATM was not involved in the damage-dependent increase in supernumerary centrosomes. Next, the effects of ATM and ATR on the centrosomes were examined by using RNA interference to silence the genes. Western blot analysis demonstrated that each protein was down-regulated by RNA interference (Figure 5C). Treatment with ATM siRNA slightly affected the cell-cycle distribution of the mutant cells, whereas treatment with ATR siRNA did not affect the distribution (Figure 5D). In accord with the finding using the ATM inhibitor, the silencing of ATM did not affect the frequency, whereas the silencing of ATR reduced the frequency from 23.3% to 14.7% ($P < 0.01$) (Figure 5E). This observation was also confirmed in HT1080 cells with Rad51C dysfunction. The silencing of ATR reduced the frequency from 11.8% to 5.8% ($P < 0.01$) (Figure 5F). These results indicate that ATR but not ATM was involved in the generation of supernumerary centrosomes. Because treatment with ATR siRNA rescued centrosome aberrations related to Rad51C depletion, ATR is likely to promote the generation of supernumerary centrosomes in the damage response signaling pathway rather than in a pathway directly associated with Rad51C.

Chk1 is involved in promoting centrosome aberrations

Since Chk1 is activated by ATR in response to DNA damage, we examined the effect of Chk1 inhibition on centrosome aberrations by treatment with the Chk1 inhibitor UCN-01 at the concentration of 100 nM in the mutant cells. This treatment reduced the frequency of centrosome aberrations from 33.0% to 19.7% ($P < 0.01$) (Figure 6A). Although UCN-01 was originally shown to inhibit Chk1 rather than Chk2, a subsequent study using GST-Cdc25C (200–256) as a substrate showed that the drug inhibited the immunoprecipitated kinase activities of Chk1 and Chk2 from wild-type HCT116 cells after exposure to ionizing radiation (25). We examined inhibition of both kinases by the drug using GST-Cdc25C (200–256) as a substrate in the mutant cells. In accord with the previous result, UCN-01 inhibited both kinases (Figure 6B). To determine which kinase is involved in the generation of supernumerary centrosomes, we examined the effect of RNA interference of the kinases on the centrosome aberrations (Figure 6C). Treatment with Chk1 or Chk2 siRNA did not affect the cell-cycle distribution of the mutant cells (Figure 5D). Silencing of Chk1 by RNA interference reduced the frequency from 30.0% to 17.3%, whereas silencing of Chk2 did not affect the frequency (Figure 6D). These results indicate that the ATR-Chk1 pathway was involved in the generation of supernumerary centrosomes.

Rad51C dysfunction promotes centrosomal accumulation of Chk1

Chk1 was shown to localize to centrosomes in response to the DNA damage induced by ultraviolet irradiation or HU treatment (26). This observation suggested that accumulation of Chk1 at centrosomes contributes to its checkpoint functions. We examined centrosomal localization of Chk1 by double immunofluorescence of Chk1 and pericentrin in HCT116 cells (Figure 6E and F). In accord with the previous report, ultraviolet irradiation or hydroxyurea treatment promoted Chk1's centrosomal localization in HCT116 cells. The frequency of cells in which Chk1 localizes to centrosomes was 12.0% in wild-type

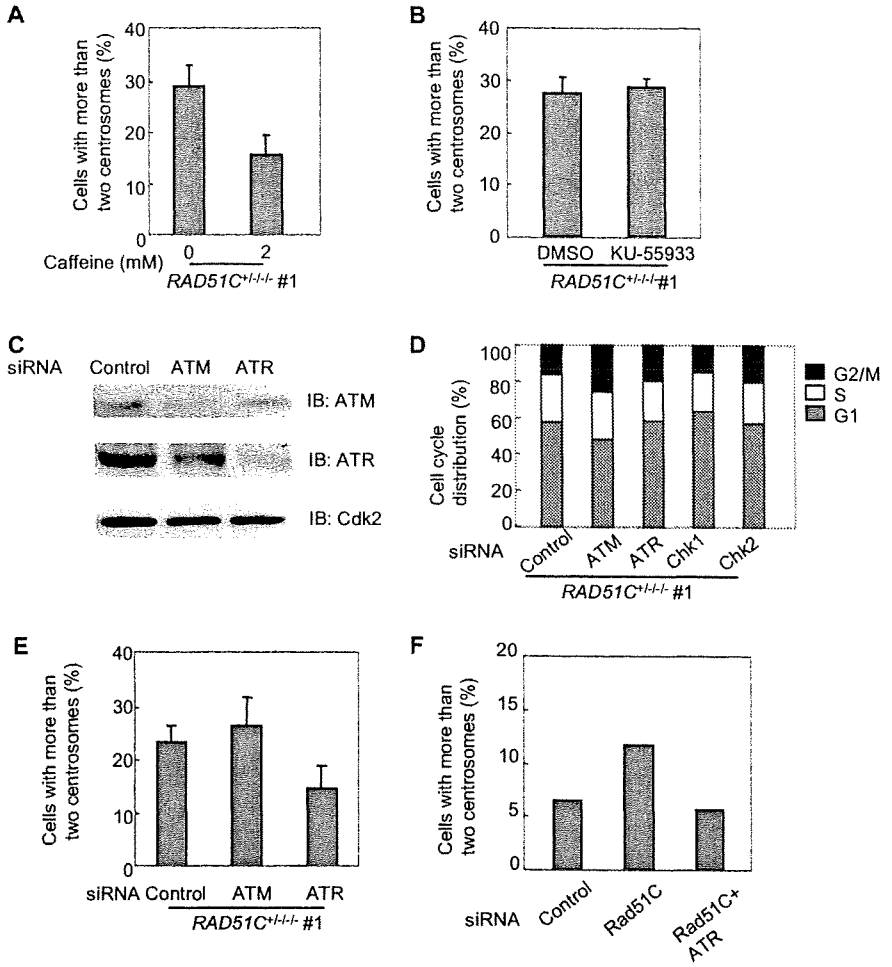

Figure 5. ATR-dependent centrosome aberrations. (**A**) Effect of caffeine treatment on centrosome aberrations in the Rad51C mutant cells. The cells were treated with 2 mM caffeine for 40 h. (**B**) Effect of an ATM inhibitor on centrosome aberrations in the Rad51C mutant cells. The cells were treated with either DMSO alone or 10 μM KU55933 dissolved in DMSO for 24 h. (C) Western blot analysis showing the expression of ATM and ATR in cells treated with siRNAs. (**D**) Cell-cycle distribution of the mutant cells treated with siRNAs. (E) Effect of silencing of ATM and ATR on centrosome aberrations in the Rad51C mutant cells. The frequencies of centrosome aberrations were examined in the cells treated with control, ATM or ATR siRNA. In (A), (B) and (E), a total of 100 cells were counted for each measurement. The results represent the means ± SEM of three independent experiments. (**F**) Effect of ATR silencing on centrosome aberrations in HT1080 cells treated with Rad51C siRNA. A total of 300 cells were counted.

cells, whereas it was 25.8% in the mutant cells ($P < 0.01$). We next examined focus formation of phosphorylated form of histone H2AX (γH2AX) in the nucleus by immunofluorescence of the protein. γH2AX is recruited to DSBs in response to DNA damage. γH2AX-positive cells were defined as cells harboring the discrete large-sized foci of the protein. The frequency of γH2AX-positive cells was 4.3% in wild-type cells, whereas it was increased to 55.7% in the mutant cells (Figure 6G). These observations indicate that Chk1 accumulates at centrosomes in response to unrepaired DNA damage caused by Rad51C dysfunction in the absence of exogenous insults. In addition, localization of Chk1 at centrosomes in response to DNA damage induced by ultraviolet irradiation or hydroxyurea treatment was promoted by Rad51C dysfunction. Together with our observation that the Rad51C mutant cells were hypersensitive to HU (Figure 2C), these results suggest that Rad51C dysfunction may lead to prolonged replication fork arrest.

Rad51C dysfunction leads to increased aneuploidy

Supernumerary centrosomes are assumed to play a role in the generation of aneuploidy by inducing aberrant chromosome segregation. The frequency of aneuploidy, characterized by one or three chromosomes, was investigated by FISH using two independent chromosome-specific centromere probes (Figure 7A). The frequencies

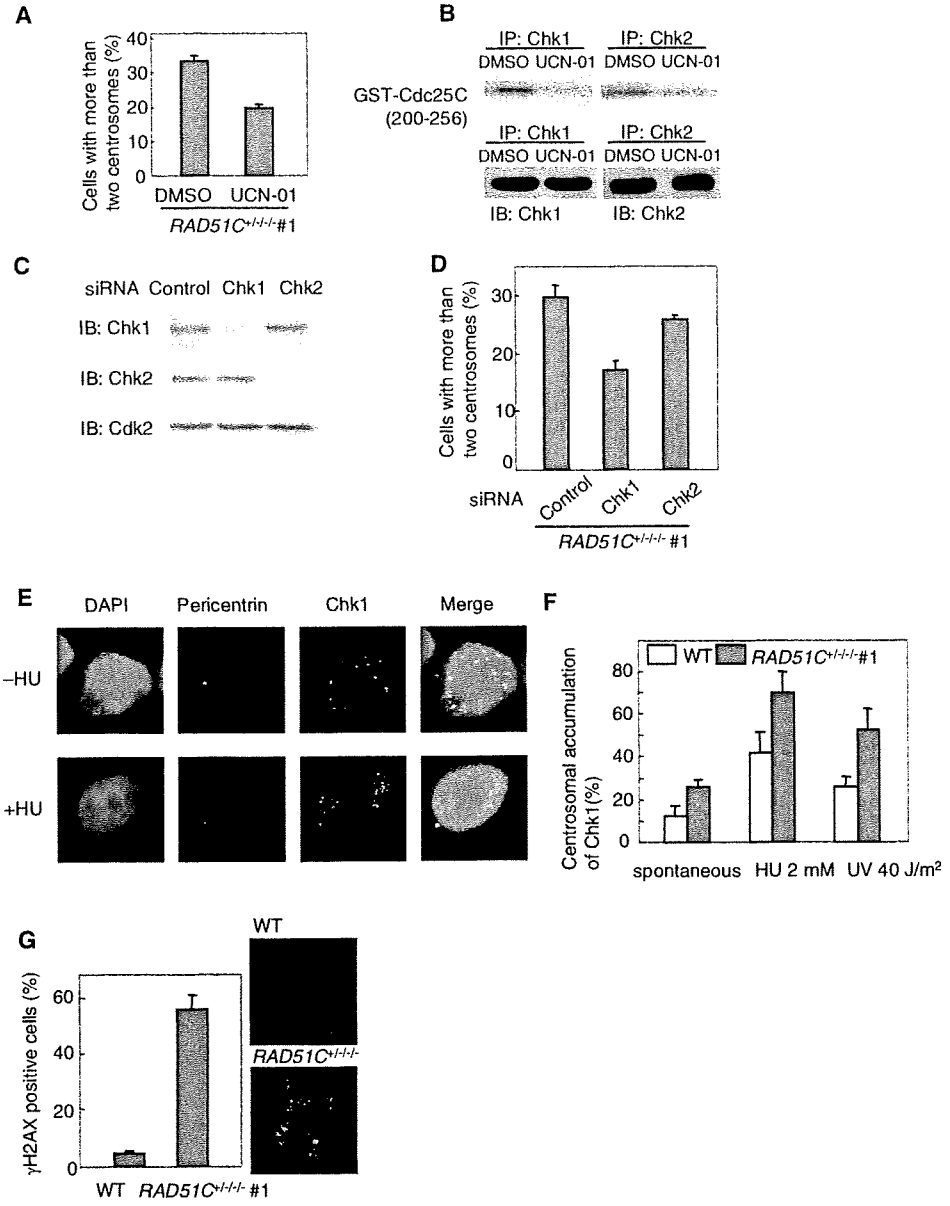

Figure 6. Chk1-dependent centrosome aberrations. (**A**) Effect of a Chk1 inhibitor on centrosome aberrations in the Rad51C mutant cells. The cells were treated with either DMSO alone or 100 nM UCN-01 dissolved in DMSO for 48 h. (**B**) Effect of UCN-01 on Chk1 and Chk2 kinase activities in the mutant cells. The cells were treated with 100 nM UCN-01 for 1 h. (**C**) Western blot analysis showing the expression of Chk1 and Chk2 in cells treated with siRNAs. (**D**) Effect of silencing of Chk1 and Chk2 on centrosome aberrations in the Rad51C mutant cells. The frequencies of centrosome aberrations were examined in the cells treated with control, Chk1 or Chk2 siRNA. (**E**) Damage-induced centrosomal accumulation of Chk1. HU treatment induces the accumulation of Chk1 at the centrosome. (**F**) Accumulation of Chk1 at the centrosome. (**G**) Focus formation of γH2AX in the nucleus. Immunofluorescence was carried out using the anti-γH2AX antibody. In (A), (D), (F) and (G), a total of 100 cells were counted for each measurement. The results represent the means ± SEM of three independent experiments.

of aneuploidy at chromosomes 7 and 17 were 3.3% and 3.4%, respectively, in wild-type cells, whereas they were increased to 7.4% and 7.6% in the Rad51C mutant cells ($P < 0.01$, Fisher's exact test) (Figure 7B). This indicates that Rad51C, like other Rad51 paralogs, maintains chromosome stability.

DISCUSSION

We have shown here that Rad51C dysfunction leads to increases in supernumerary centrosomes in an ATR-Chk1-dependent manner and to aneuploidy in human cells. This observation indicates that the DNA